

AD-A208 688

Pulsed Photolytic Density Scaling Experiment for BiF

J. F. BOTT, C. E. GARDNER, R. F. HEIDNER,
J. M. HERBELIN, R. HOFLAND, JR., J. S. HOLLOWAY,
J. B. KOFFEND, M. A. KWOK, R. H. UEUNTEN,
S. T. AMIMOTO, and G. N. HARPER

Aerophysics Laboratory
Laboratory Operations
The Aerospace Corporation
El Segundo, CA 90245

1 May 1989

Prepared for

AIR FORCE WEAPONS LABORATORY
Kirtland Air Force Base, NM 87117

SPACE SYSTEMS DIVISION
AIR FORCE SYSTEMS COMMAND
Los Angeles Air Force Base
P.O. Box 92960
Los Angeles, CA 90009-2960

APPROVED FOR PUBLIC RELEASE;
DISTRIBUTION UNLIMITED

DTIC
ELECTE
JUN 06 1989
S H D

89 6 05 166

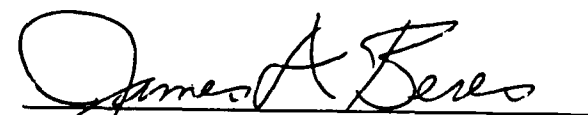
This report was submitted by The Aerospace Corporation, El Segundo, CA 90245, under Contract No. F04701-88-C-0089 with the Space Systems Division, P.O. Box 92960, Los Angeles, CA 90009-2960. It was reviewed and approved for The Aerospace Corporation by W. P. Thompson, Director, Aerophysics Laboratory. Lt. Scott Levinson, SD/CNID, was the Air Force project officer.

This report has been reviewed by the Public Affairs Office (PAS) and is releasable to the National Technical Information Service (NTIS). At NTIS, it will be available to the general public, including foreign nationals.

This technical report has been reviewed and is approved for publication. Publication of this report does not constitute Air Force approval of the report's findings or conclusions. It is published only for the exchange and stimulation of ideas.



SCOTT W. LEVINSON, Lt, USAF
MOIE Project Officer
SD/CNID



JAMES A. BERES, Lt Col, USAF
Director, AFSTC West Coast Office
AFSTC/WCO

UNCLASSIFIED

SECURITY CLASSIFICATION OF THIS PAGE

REPORT DOCUMENTATION PAGE

1a. REPORT SECURITY CLASSIFICATION Unclassified			1b. RESTRICTIVE MARKINGS		
2a. SECURITY CLASSIFICATION AUTHORITY			3. DISTRIBUTION/AVAILABILITY OF REPORT Approved for public release; distribution unlimited.		
2b. DECLASSIFICATION/DOWNGRADING SCHEDULE					
4. PERFORMING ORGANIZATION REPORT NUMBER(S) TR-0088(3604)-2			5. MONITORING ORGANIZATION REPORT NUMBER(S) SD-TR-89-31		
6a. NAME OF PERFORMING ORGANIZATION The Aerospace Corporation Laboratory Operations		6b. OFFICE SYMBOL (If applicable)	7a. NAME OF MONITORING ORGANIZATION Space Systems Division Air Force Systems Command		
6c. ADDRESS (City, State, and ZIP Code) 2350 E. El Segundo Blvd. El Segundo, CA 90245				7b. ADDRESS (City, State, and ZIP Code) Los Angeles Air Force Base P.O. Box 92960 Los Angeles, CA 90009-2960	
8a. NAME OF FUNDING/SPONSORING ORGANIZATION Air Force Weapons Laboratory		8b. OFFICE SYMBOL (If applicable)	9. PROCUREMENT INSTRUMENT IDENTIFICATION NUMBER F04701-88-C-0089		
8c. ADDRESS (City, State, and ZIP Code) Kirtland Air Force Base, N. Mex. 87117		10. SOURCE OF FUNDING NUMBERS			
		PROGRAM ELEMENT NO.	PROJECT NO.	TASK NO.	WORK UNIT ACCESSION NO.
11. TITLE (Include Security Classification) PULSED PHOTOLYTIC DENSITY SCALING EXPERIMENT FOR BiF					
12. PERSONAL AUTHOR(S) J. F. Bott, C. E. Gardner, R. F. Heidner, J. M. Herbelin, R. Hofland, et al.					
13a. TYPE OF REPORT		13b. TIME COVERED FROM TO		14. DATE OF REPORT (Year, Month, Day) 1989 May 1	
				15. PAGE COUNT 77	
16. SUPPLEMENTARY NOTATION 10 to the 11th power (CC) Keywords:					
17. COSATI CODES			18. SUBJECT TERMS (Continue on reverse if necessary and identify by block number)		
FIELD	GROUP	SUB-GROUP	Chemical Lasers		
			Bismuth Fluoride		
			Trimethyl Bismuth		
			Nitrogen Fluoride		
19. ABSTRACT (Continue on reverse if necessary and identify by block number) <u>Hydrogen</u> <u>61 Delta</u> <u>Krypton Fluoride</u>					
<p>A large volume density scaling experiment has been devised and conducted for BiF(AO₂) generated by the energy storage molecule NF(a₁). Kr⁺ excimer laser photolysis has been used to initiate reactive mixtures of NF₂, H₂, and trimethyl bismuth (TMB). The goals of the experiment are to perform density scaling in BiF(AO₂) to the level of measurable gain and to identify and study kinetics issues in the elevated density regime. The BiF(AO₂) density observed to date is around 10¹⁸ molecules/cm³, somewhat lower than reported by Herbelin using electrical discharge initiation of similar mixtures, and substantially lower than was predicted.</p> <p>The yield of NF(a₁) from NF₂ photolysis determined by absolute radiometry is lower than that predicted on the basis of previous NF₂ photolysis experiments. An incomplete understanding of the photophysics of NF₂ for long-pulse laser photolysis or possible errors in the absolute calibration of the photomultiplier are two possible explanations of this discrepancy.</p>					
20. DISTRIBUTION/AVAILABILITY OF ABSTRACT <input type="checkbox"/> UNCLASSIFIED/UNLIMITED <input checked="" type="checkbox"/> SAME AS RPT <input type="checkbox"/> DTIC USERS			21. ABSTRACT SECURITY CLASSIFICATION Unclassified		
22a. NAME OF RESPONSIBLE INDIVIDUAL			22b. TELEPHONE (Include Area Code)		22c. OFFICE SYMBOL

SECURITY CLASSIFICATION OF THIS PAGE

19. ABSTRACT (Continued)

Modeling and analysis show that the low result cannot be explained solely by transmission losses in the KrF optical train or by incomplete thermal dissociation of N_2F_4 .

The low $BiF(AO^+)$ density observed in the experiment can result from the absolute calibration of the photomultiplier and its optical configuration. Another source of uncertainty is the photophysics of TMB under the influence of the present high-power, long-pulse excimer laser. Nonlinear absorption by the TMB may attenuate the laser pulse before it reaches the part of the cell being monitored and thus alternate initiation techniques may be required.

$BiF(AO^+)$ vibrational and rotational temperatures have been observed for several conditions, and the dependence of the $[BiF(A)]$ on TMB and SF_6 has been measured. The predicted usefulness of SF_6 as a high heat capacity diluent for controlling heat release has been demonstrated. A large ground state $BiF(XO^+)$ density has been observed by self-absorption techniques.

500 1110
1000 1000
1000 1000

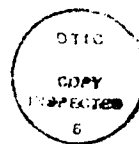
UNCLASSIFIED

SECURITY CLASSIFICATION OF THIS PAGE

B

PREFACE

The authors would like to acknowledge the generous support of the Air Force Weapons Laboratory (ARBI Branch). In particular, we recognize the encouragement given by Dr. P. V. Avizonis and Capt. G. P. Perram. This work was supported by AFWL under AFSD Contract F04701-88-C-0089.



Accession For	
NTIS GRA&I	<input checked="checked" type="checkbox"/>
DTIC TAB	<input type="checkbox"/>
Unannounced	<input type="checkbox"/>
Justification	
By	
Distribution/	
Availability Codes	
Dist	Avail and/or Special
A-1	

CONTENTS

PREFACE	1
I. INTRODUCTION.....	9
II. EXPERIMENTAL PROCEDURES.....	13
A. Apparatus Design.....	13
B. Medium Diagnostics.....	18
C. KrF Excimer Laser.....	20
D. Ultraviolet Photon Injection.....	23
E. Optical Calibrations.....	25
F. Oven Uniformity Studies.....	32
G. KrF Laser Mirror Evaluation and Cell Window Transmission.....	32
III. KINETICS AND SPECTROSCOPY EXPERIMENTS.....	37
A. Photometric Measurements of BiF(A,v=0) and NF(a ¹ Δ)	37
B. NF ₂ Absorption Measurements.....	45
C. OMA Measurements of BiF Rotational and Vibrational Temperatures.....	47
D. OMA Measurements of the BiF Ground State Density.....	48
E. Effect of SF ₆ Scaling.....	52
F. Effect of Scaling of All Reagents on BiF A State Population.....	55
G. Effect of TMB Variations.....	63
H. Comments on the Measurements.....	63

CONTENTS (continued)

IV.	MODELING CALCULATIONS.....	67
	A. Modeling of the Photolysis of the N_2/F_4 Argon Mixture.....	67
	B. Modeling of the Photolysis of the Laser Mixture.....	68
V.	ASSESSMENT AND DISCUSSION.....	79
	REFERENCES.....	81

FIGURES

1.	Main Experiment Schematic.....	14
2.	BiF(A) and BiF(X) Production vs. Fraction of NF ₂ Photolyzed.....	17
3.	KrF Laser Output.....	22
4.	Schematic of Optical Train for Transverse Laser Photolysis.....	24
5.	Schematic of Optical Train for Collinear Laser Photolysis.....	27
6.	Calibration Schematic - Reference Approach.....	29
7.	Absorption by NF ₂	31
8a.	Schematic for Laser Mirror Reflectance Measurements.....	33
8b.	Schematic for Absolute Reflectance Measurements.....	34
9.	Photomultiplier Trace of BiF(A) Emission.....	38
10.	NF(a ¹ Δ) Emission from the N ₂ F ₄ /Argon Mixture.....	40
11.	OMA Measurements and Simulation of the (0,0) Band of BiF(A) for Rotational Temperature Determination.....	49
12.	OMA Spectrum and Simulation of the BiF(A) Emission.....	50
13.	OMA Emission Spectrum of BiF(A) at Different Delay Times.....	51
14.	OMA Measurements of "End-on" BiF(A) Emission and Simulation of the "Band Distortion".....	53
15.	Sensitivity of BiF(A) Spectrum Simulations for Different Values of BiF(X).....	54
16.	Integrated BiF(0,2) Emission vs. SF ₆ Density.....	57
17.	Peak BiF(0,2) Emission vs. SF ₆ Density.....	58
18.	BiF A State Density (Peak) vs. SF ₆	59
19.	BiF A State Density (Integrated) vs. SF ₆	60
20.	Peak BiF(0,2) Emission vs. Total Pressure.....	61
21.	Integrated BiF(0,2) Emission vs. Total Pressure.....	62

FIGURES (continued)

- 22. Integrated BiF(0,2) Emission vs. TMB Density (Reproduced from
Ref. 10.)..... 64
- 23. Modeling Predictions of Peak BiF(A) and BiF(X) Densities vs.
Initial Bismuth Atoms..... 74

TABLES

1.	Operating Conditions for Runs N11126 and N31121.....	19
2.	Operating Parameters for Excimer Laser (KrF) Facility.....	21
3.	Comparison of Transverse and Collinear KrF Laser Pumping.....	26
4.	BiF(A) and NF($a^1\Delta$) Density Calculations.....	41
5.	NF($a^1\Delta$) and BiF(A, $v=0$) Determinations.....	43
6.	Parameters for Measurement of BiF(A) Relative to NF($a^1\Delta$).	46
7.	Temperature Variation with Added SF ₆	56
8.	BiF A State Density with Added SF ₆	56
9.	BiF A State Density with Total Reagent Scaling.....	56
10.	Kinetic Model for Production of NF($a^1\Delta$).	69
11.	Kinetic Processes Involving Bi and BiF.....	70
12.	Sample Code Calculation for "Laser Mixture".....	73

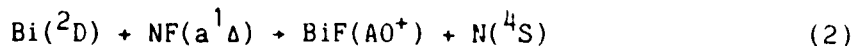
I. INTRODUCTION

Early work by Herbelin and Conen¹ showed that



had a fast overall reaction rate at room temperature ($k_1 = 1.5 \times 10^{-11} \text{ cm}^3/\text{molecule-sec}$)² with a high yield of $\text{NF}(\text{a}^1\Delta)$, the first excited electronic state of the molecule. A branching ratio (k_{1b}/k_1) greater than 90% in $\text{NF}(\text{a}^1\Delta)$ was indirectly inferred by Malins and Setser,² and by Cheah and Clyne.³ Given the metastability of $\text{NF}(\text{a}^1\Delta)$, this unusual result suggests the prospect of an electronic state inversion. This idea was explored by Capelle et al.,⁴ who observed an $\text{NF}(\text{a}^1\Delta)$ -pumped population inversion in the bismuth atom, $\text{Bi}(\text{}^2\text{D})$, with respect to $\text{Bi}(\text{}^4\text{S})$. Further work was pursued by Herbelin et al. in a subsonic⁵ and a supersonic⁶ flow facility in which bismuth metal was injected from a heater or via a flow of gaseous trimethyl bismuthine (TMB): $\text{Bi}(\text{CH}_3)_3$. These efforts and further flow tube investigations showed that the density scaling of excited $\text{Bi}(\text{}^2\text{D})$ reached a kinetically controlled limit.

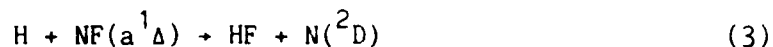
Studies by Herbelin and Klingberg⁷ and by Herbelin⁸ indicated that at sufficiently high $\text{NF}(\text{a}^1\Delta)$ and $\text{Bi}(\text{}^2\text{D})$ densities, the excited atom was removed by participation in the reaction



which occurred with a fast rate. The possibility of density scaling $\text{BiF}(\text{A})$ was then proposed, which would lead to population inversions on selected $\text{BiF}(\text{A} \rightarrow \text{X})$ rovibronic transitions. Careful laser-induced fluorescence studies by Heidner et al.^{9a,9b} of the $\text{BiF}(\text{A}^0+)$ radiative decay and collisional quenching behavior supported these prospects. Chemical kinetics of

the $\text{NF}(a^1\Delta)/\text{BiF}$ system were further surveyed in reports by Koffend and Heidner¹⁰ and by Bott.¹¹

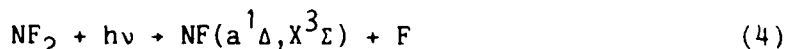
Using a KrF excimer laser at 249 nm, Koffend et al.¹² were able to photodissociate NF_2 as a source of F atoms to initiate the $\text{H}_2\text{-NF}_2$ chemical chain reaction. With this approach, they were able to determine the quantum yield of $\text{NF}(a^1\Delta)$ production by Reaction (1) as well as rates for $\text{F} + \text{NF}_2$ three body recombination, quenching of $\text{NF}(a^1\Delta)$ by NF_2 , and quenching of $\text{HF}(v)$ by NF_2 . Preliminary $\text{NF}(a^1\Delta)$ density scaling attempts in this small volume showed promise. Critical to the success of scaling $\text{NF}(a^1\Delta)$ is the fact that Reaction (1) has been found to be 50 times faster than the secondary process



which has a rate coefficient of $k_3 \sim 3 \times 10^{-13} \text{ cm}^3/\text{molecule-sec}$. In a subsequent study, Heidner et al.¹³ obtained a high resolution absorption spectrum of NF_2 around 250 nm and determined the quantum yield of $\text{NF}(a^1\Delta)$ from NF_2 photodissociation between 240 and 270 nm. The quantum yield of F from NF_2 was not measured in any of these studies, although recent work in the Aerophysics Laboratory suggests this yield is unity.

The totality of these efforts gave impetus to the concept that a clean, well defined, large volume density scaling experiment might be conducted using pulsed KrF excimer laser photolysis to initiate an $\text{NF}_2/\text{H}_2/\text{TMB}$ mixture by generating the needed F atoms from the photolysis of NF_2 and the required Bi atoms from the photolysis of TMB. The objectives of this experiment were to conduct density scaling of the $\text{NF}(a^1\Delta)$ and $\text{BiF}(A0^+)$ molecules, to generate measurable gain in the vibrational and rotational manifold of the $\text{BiF}(A0^+ \rightarrow X0^+)$ band system, and to identify and study kinetics issues arising from the elevated densities of the relevant species. The ultimate goal of this effort was to provide a BiF laser demonstration near 450 nm.

A pulsed, premixed, photolytic experiment was then designed. The premixed condition implied that the necessary bismuth source (i.e., TMB) must exist in the vapor phase. The combustion stability of NF_2/H_2 mixtures at the elevated cell temperatures necessary to generate NF_2 from N_2F_4 became an issue. Fortunately, TMB helps to serve as a moderator and radical scavenger in these mixtures. To extend the useful range of pressure, temperature, and stoichiometry, the experiment was designed as a slowly flowing system to minimize dwell time for $\text{N}_2\text{F}_4/\text{H}_2$ mixtures in the cell. From modeling calculations, optimal gain was shown to be achieved at low temperatures (i.e., less than or equal to the oven temperature). High heat capacity diluents such as SF_6 were therefore chosen to minimize the temperature rise caused by heat release in Reactions 1, 3, 5, and subsequent secondary reactions. As previously described, F atoms were produced photolytically by the KrF laser ($t \leq 0.3 \mu\text{sec}$) and consumed by the well-known reaction with hydrogen to produce H atoms:



Although some augmentation and regeneration of F atoms by $\text{NF} + \text{NF}_x$ reactions does occur, the principal source of F (and therefore H) was Reaction (4). This photoinitiation requirement, the cell geometry, and the cell volume determined the energy of the KrF laser. Accordingly, an electron beam pumped KrF laser providing over 30 J/pulse was used. Both transverse and collinear ultraviolet photon pumping geometries were explored.

The experimental diagnostics were designed to determine absolute number densities of $\text{NF}(a^1\Delta)$, $\text{BiF}(A0^+)$, $\text{BiF}(X0^+)$ and the vibrational, rotational, and static temperatures as a function of time, pressure, stoichiometry, and KrF laser fluence. These measurements establish density scaling laws, provide kinetics data, and allow estimates of optical gain. Secondary diagnostics supported detector calibrations, mirror reflectance

evaluations, and degree of N_2F_4 dissociation to NF_2 . KrF laser pulse shape and fluence were also monitored. Spectral measurements of the molecular bands were made using a high resolution optical multichannel analyser system. Because the modeling predicted sufficient optical gain, a BiF resonator and associated laser diagnostics were developed.

In Section II, the experimental approach and apparatus will be discussed. The kinetics and spectroscopy experiments will be described in Section III. The modeling effort that aided experimental design and supported data interpretation is presented in Section IV. Our assessment and discussion of the results are given in Section V.

II. EXPERIMENTAL PROCEDURES

The experimental apparatus and schematic are discussed herein. Because of the requirement to establish unambiguously the absolute number densities of BiF(A) and BiF(X) , unusual care was applied to density calibrations. Several auxiliary experiments, tests, and calibrations were designed to verify the measurements and define their uncertainties. These included both relative and absolute end-to-end responsivity calibrations at two wavelengths for the principal photomultiplier detector system. In addition, we performed the following procedures: an absolute intensity calibration of the optical multichannel analyzer; absorption measurements of NF_2 in the test cell and gas temperature uniformity measurements; optical filter transmission checks; ultraviolet mirror reflectance measurements; and digital flowmeter calibrations.

A. APPARATUS DESIGN

As shown in Fig. 1, the schematic of the main experiment, the setup consists of a cylindrical suprasil cell approximately 120 cm in length between the Brewster angle window mounts. The latter accommodate linearly polarized 457 nm radiation (vertical polarization axis) through calcium fluoride or sapphire windows. Suprasil was chosen as the cell material to minimize fluorescence induced by the ultraviolet photon flux needed for chemical photoinitiation. The clear aperture is 2 cm in diameter, although the body of the tube over most of its length is slightly over 4 cm i.d. During operation, a steady flow of reagents through the cell was developed at a nominal plug flow velocity of 100 cm/sec to minimize wall reactions that might catalyze the decomposition of the mixture. Cell pressure was set by a downstream throttling valve leading to a vacuum forepump capable of better than 50 μm evacuation pressure; pressure was read using MKS Baratron gauges. To prevent prereaction of N_2F_4 or NF_2 with H_2 , mixing of reagents occurs at the upstream entrance to the tube. The main flow consisting of a 10:1 $\text{Ar:N}_2\text{F}_4$ mixture, or the mixture plus a high heat capacity

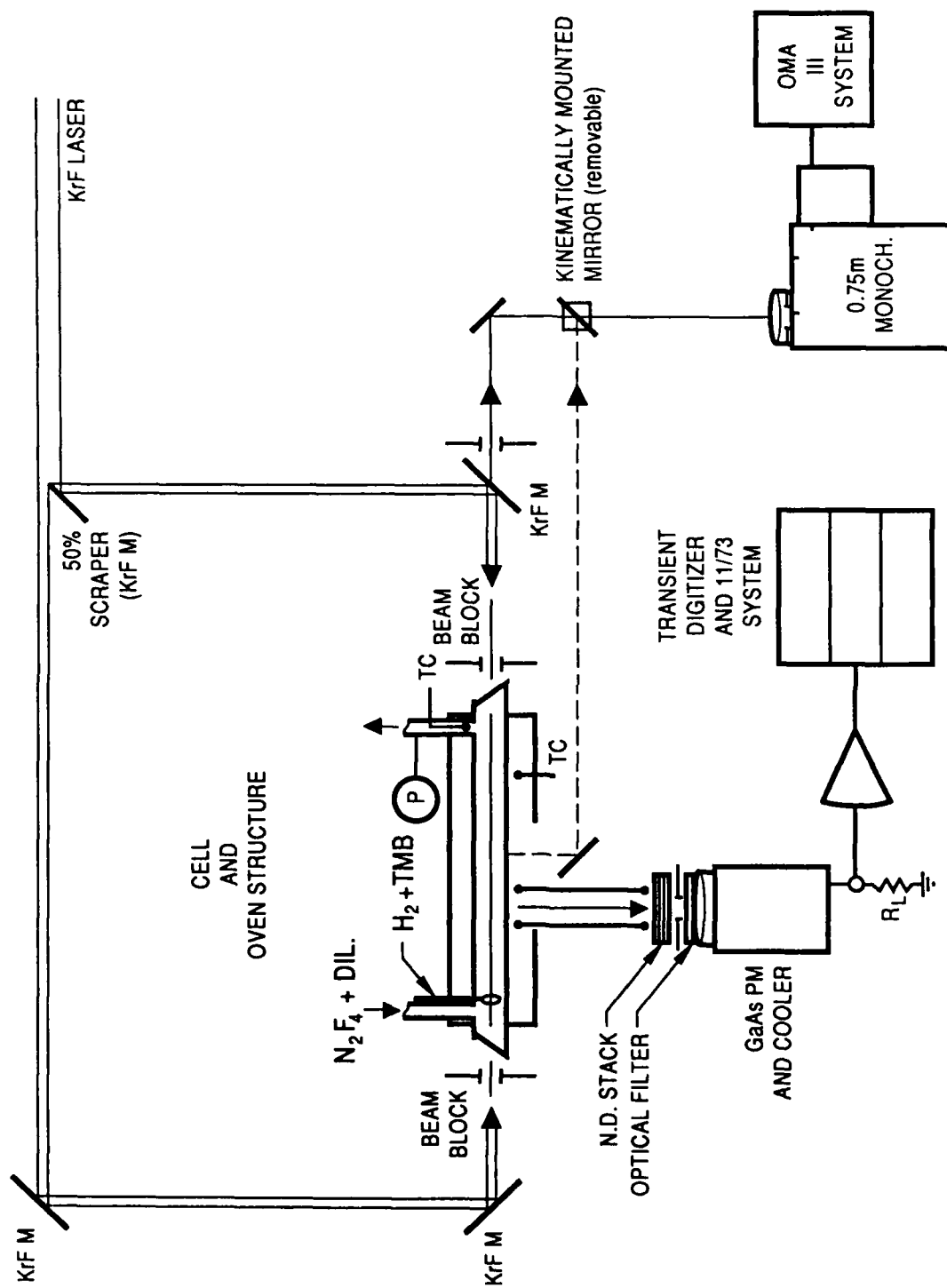


Fig. 1. Main Experiment Schematic.

diluent such as SF₆, enters the tube through a 0.5 cm diameter sidearm. Hydrogen, the TMB + Ar mixture, and additional diluent enter the tube through eight holes in a suprasil ring injector. Flowrates of all reagents are monitored with Tylan digital flow meters.

The flow cell is enclosed in an oven structure (Watlow, Inc.) with three heating strips embedded in the bottom panel of the rectangular oven box. The cell passes through the end walls of the oven, permitting the Brewster windows to remain in ambient air. About 85 cm of the central part of the cell length is heated to the elevated temperature. One side of the oven incorporates a long rectangular slot used for side viewing or for transverse ultraviolet irradiation of the cell. Optimum uniform heating required that this slot be sealed until test time. A typical cell gas temperature was 150°C as determined by a thermocouple placed in the exhaust sidearm of the flow, although temperatures as high as 200°C could be reached. The purpose of the oven was the thermal dissociation of N₂F₄:

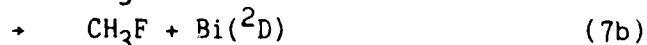
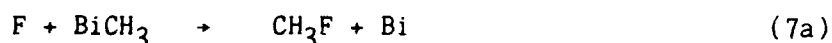


The 248 nm KrF excimer laser beam was directed into the cell with the collinear geometry shown in Fig. 1, in which the collimated KrF beam is split into two legs for opposed injection into the cell. Aperture stops permitted 2.0 or 2.5 cm diameter beams to enter the cell. Opposed injection provides a more uniform axial laser flux distribution. A typical flux per leg is 700 kW-cm⁻² whereas fluxes range from 300 to 1100 kW-cm⁻². Collinear injection was chosen mainly to overcome the problem of long-lived cell wall fluorescence caused by transverse injection. Transverse injection obliterated useful side or end diagnostics signals. The choice of collinear versus transverse injection of ultraviolet radiation is discussed further herein.

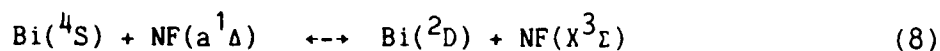
The photodissociation of NF₂ should provide a nearly instantaneous source of F atoms, based on its nearly structureless absorption continuum. However, NF(a¹Δ) has been shown to exhibit a substantial induction

time ($\sim 80 \mu\text{s}$) for production from NF_2 photolysis.^{12,13} Subsequently, other experiments in the Aerophysics Laboratory have shown that there is no induction time in the NF_2 photolysis channel (Q.Y. $\approx 93\%$) leading to $\text{F} + \text{NF}(\text{X})$. This is consistent with time-resolved titration measurements of F atoms with HCl . Thus, the reaction sequence of (5) followed by (1) creates $\text{NF}(\text{a}^1\Delta)$ on a rapid time scale. As suggested by Fig. 2, 50% photodissociation of NF_2 approximates the optimum operating condition where NF_2 supplies one reagent to Reaction (1) and its photofragments generate the other.

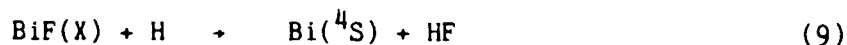
The liberation of free bismuth atoms can occur by many channels. Typical TMB concentrations are 1 to 10% of NF_2 or H_2 densities such that TMB is really a trace constituent in the flow. Some TMB photodissociation can occur at 248 nm with undefined secondary photolytic channels that eventually lead to free Bi. Indeed, Koffend and Heidner¹⁰ showed that $\text{Bi}({}^2\text{D})$ is produced at $t = 0$ while $\text{Bi}({}^4\text{S})$ grows in at later times. It is also likely that F atoms will attack CH_3 radicals and successively strip the TMB molecule and its photofragments by reactions such as:



The dominant channel is undetermined, but the experimental results reported here may suggest some possibilities. Ground state bismuth atoms are excited rapidly by the near-resonant process⁴



and the $\text{Bi}({}^2\text{D})$ reacts further with $\text{NF}(\text{a}^1\Delta)$ according to Reaction (2). Herbelin has suggested that H atoms can recycle BiF into Bi by



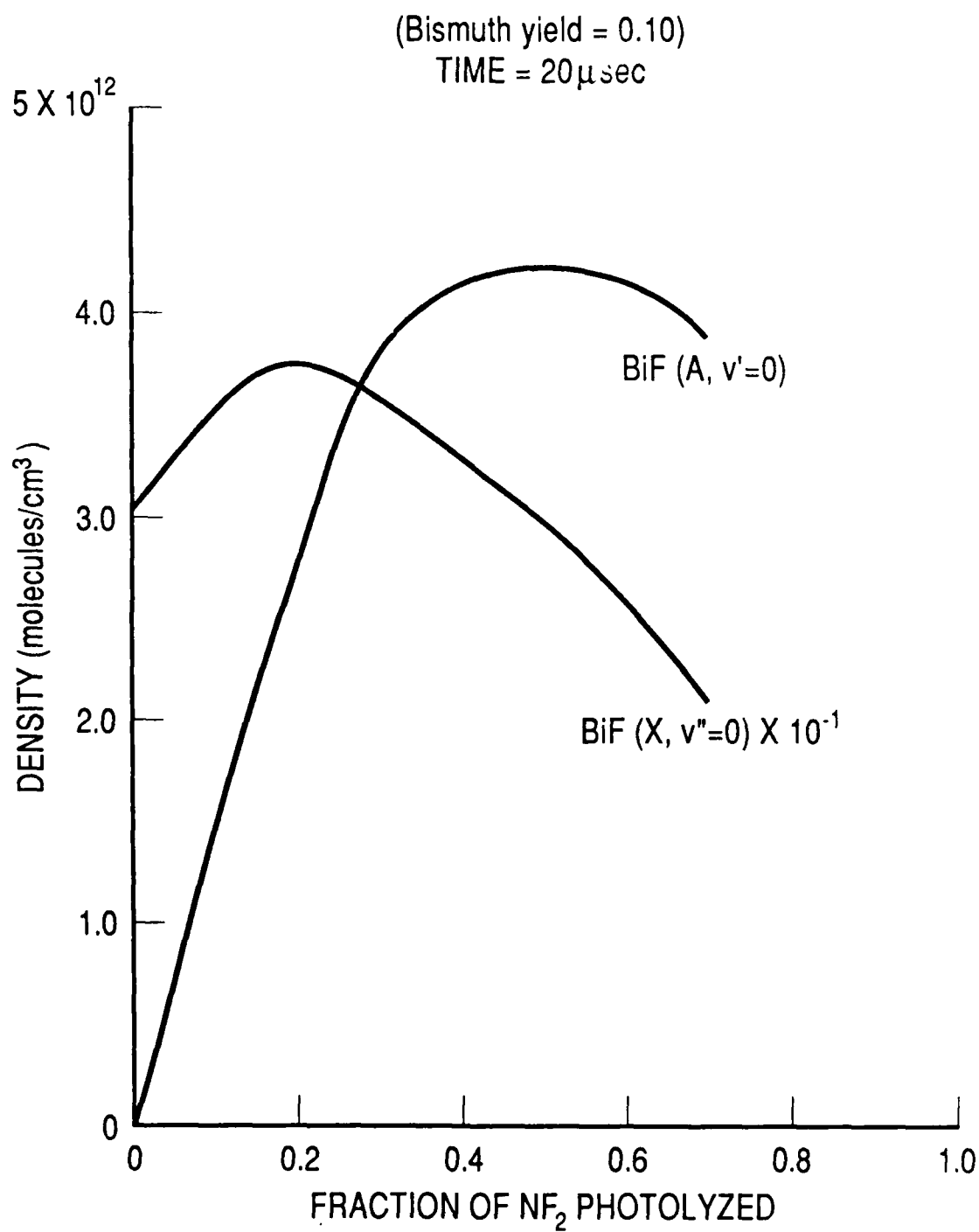


Fig. 2. BiF(A) and BiF(X) Production vs. Fraction of NF₂ Photolyzed.

Reaction (9) will only work efficiently to remove BiF(X) on the proper time scale in the condition of high H atom densities. Other recycling possibilities exist.

A typical run condition is summarized in Table 1. BiF(A) densities and estimated gains can be computed on the basis of 100% use of bismuth atoms. It can be seen that this experiment could provide a demonstration of measurable gain (or lasing) if the modeling calculations are accurate. Since this condition is predicated on the assumption of high bismuth utilization and the ability to surmount potential prereaction problems, several medium diagnostics were applied to these experiments to extract valuable density and kinetic information under a variety of operating conditions.

B. MEDIUM DIAGNOSTICS

Two principal optical diagnostics are used in these tests. The first is a submicrosecond response, cooled GaAs photomultiplier tube arranged to observe side light emission during the photolysis and subsequent chemical reactions (Fig. 1). The optical volume defined by a lens is the product of the depth across the tube diameter and a nominal 2.3×4.3 cm cross section along the tube axis. The lens is aperture-stopped to define the solid angle. A rear mirror structure internal to the oven provides some signal enhancement. Emissions at 874 and 457 nm are detected selectively using very narrowband optical filters with bandwidths of 0.4 and 1.0 nm, respectively. The NF(a+X) band emission at 874 nm provides data on $\text{NF(a}^1\Delta)$ as a function of time. Unfortunately, interfering N_2 first positive emissions prevented the use of this wavelength detector during photolysis of the mixtures containing H_2 . The 457 nm radiation represents time-dependent emission from the $\text{BiF(A} \rightarrow \text{X, } v'=0, v''=2)$ band. In the temperature range of study, both spectral band shapes are essentially constant, and no corrections are applied to the data. Photomultiplier signals were passed through a linear amplifier providing gains up to 100x, recorded by a LeCroy 2264 analog-to-digital waveform digitizer in a CAMAC crate, and transferred to a DEC 11/73 microcomputer system. Two types of calibrations were conducted

Table 1. Operating Conditions for Runs N11126 and N31121

Run N11126

Averages = 1; No. of Channels = 1; NPTS : 700

25 points with period 1.0 μ sec
 675 points with period 0.5 μ sec
 0 points with period 1.0 μ sec

Specie	Flow Read	Fraction	Flow Cal	Flow	Pressure	Concentration
N ₂ F ₄	198.00	0.100	1.0490	1.87	0.034	0.78092E+15
NF ₂				37.80	0.688	0.15811E+17
TMB	190.00	0.023	0.2880	1.32	0.024	0.55413E+15
H ₂	27.00	1.000	1.1620	31.41	0.572	0.13137E+17
Ar	29.00	1.000	1.5550	234.34	4.265	0.98016E+17
SF ₆	1510.00	1.000	0.2880	447.72	8.148	0.18727E+18

Inlet temperature: 147; outlet temperature: 147; oven temperature: 147

Pressure: 13.730; plug flow (cm/sec): 105.213

Laser power (J): 0.600

Run N31121

Averages: = 1; No. of Channels = 1; NPTS : 700

25 points with period 1.0 μ sec
 675 points with period 1.0 μ sec
 0 points with period 1.0 μ sec

Specie	Flow Read	Fraction	Flow Cal	Flow	Pressure	Concentration
N ₂ F ₄	184.00	0.100	1.0490	1.57	0.055	0.12332E+16
NF ₂				35.46	1.252	0.27846E+17
Ar	0.00	1.000	1.5550	173.69	6.133	0.13641E+18

Inlet temperature: 161; outlet temperature: 161; oven temperature: 300

Pressure: 7.440; plug flow (cm/sec): 56.036

Laser Power (J): 0.480

to deduce absolute number densities for $\text{NF}(a^1\Delta)$ and $\text{BiF}(A)$. These calibrations are discussed herein.

The second diagnostic is the optical multichannel analyser (OMA III) used to observe both side light and end-on emissions. The device was mounted on a McPherson 0.75 m Czerny-Turner monochromator that could provide a minimum wavelength resolution of 1.5 \AA . The wavelength range covered is 420 to 480 nm. There are several bands of the $\text{BiF}(A \rightarrow X)$ system in this region that can provide vibrational and rotational temperature data as well as the total density of $\text{BiF}(A0^+)$. Comparison of end-on and side light results can provide some indication of self-absorption, and therefore, some measure of ground state $\text{BiF}(X0^+)$ vibrational densities. An absolute radiance calibration was conducted on the OMA system. The optical trains were set up to avoid moving the monochromator. As suggested in Fig. 1, only one mirror, kinematically mounted, needs to be removed to perform an end-on observation. The 50 mm Nikkor lens on the monochromator is adjusted to provide a magnified entrance slit image in the center of the cell. For the end-on train, two variable aperture stops plus the lens stop serve to define the optical volume ($w = 3.3 \text{ mm}$; $h = 7.8 \text{ mm}$) along the tube axis and the very small solid angle ($\Omega = 1.7 \times 10^{-6}$).

The performance of the KrF laser is recorded by an energy meter sampling the 6% of the beam that is reflected off a CaF_2 wedge. The time-dependence of the laser pulse and E-beam current are recorded on an oscilloscope. The collimation and spatial quality of the beam are qualitatively verified using laser irradiation on photographic film.

As previously discussed, cell pressure, exhaust gas temperature, and flow rates of all initial species are recorded for each test.

C. KrF EXCIMER LASER

The KrF excimer laser is a single-sided electron-beam-pumped, 7 liter device using typical room temperature mixtures of argon, 0.5% fluorine, and 5% krypton, as summarized in Table 2. The pulse length is 0.7 μsec and the

Table 2. Operating Parameters for Excimer Laser (KrF) Facility
(Argon, 0.5% Fluorine, 5% Krypton)
Existing (June 5, 1986)

Cell densities	1.3 - 2.0	(Amagat)
E-beam voltage	350	(kV)
Current density	10 - 40	(amps/cm ²)
E-beam pulse duration	0.2 - 1.5	(μ s)
B-field at cathode	0.6 \pm 0.1	(K Gauss)
B-field at cell	1.3 \pm 0.1	(K Gauss)
Cell volume	~ 5.5 (B-field uniformity)	(ℓ)
Unstable confocal resonator output coupling fraction	0.5	
Beam shape at magnification = 1.41	8 \times 8 with 5.6 \times 5.6 obscuration	(cm ²)
Laser energy	20 (at 20/Psia)	(J/pulse)
Specific energy	~ 3.6	(J/ ℓ)

pulse shape is nearly top hat or rectangular (Fig. 3). The off axis confocal resonator is set up to produce a collimated beam with a U-shaped cross section displaying a rectangular base approximately 4 \times 8 cm with protruding "fangs," each approximately 5 \times 1.5 cm that are removed by scrapers. A CaF₂ beam-splitter and an 8-in. Scientech calorimeter were used to measure laser output energy on each shot. Total deliverable energy in the base cross section can approach 20 to 24 joules yielding maximum fluences of 0.6 to 0.8 J/cm². Typical energies in the rectangular base are 13 to 15 J. The laser wavelength is 248.5 nm, with a bandwidth on the order of 0.1 nm. The light is randomly polarized. In this facility, laser pulses can be repeated within 5 min.; the laser mixture needs to be changed every 15 to 20 shots. An available telescope, which could enhance the fluence up to 9 \times , was not used in this set of experiments.

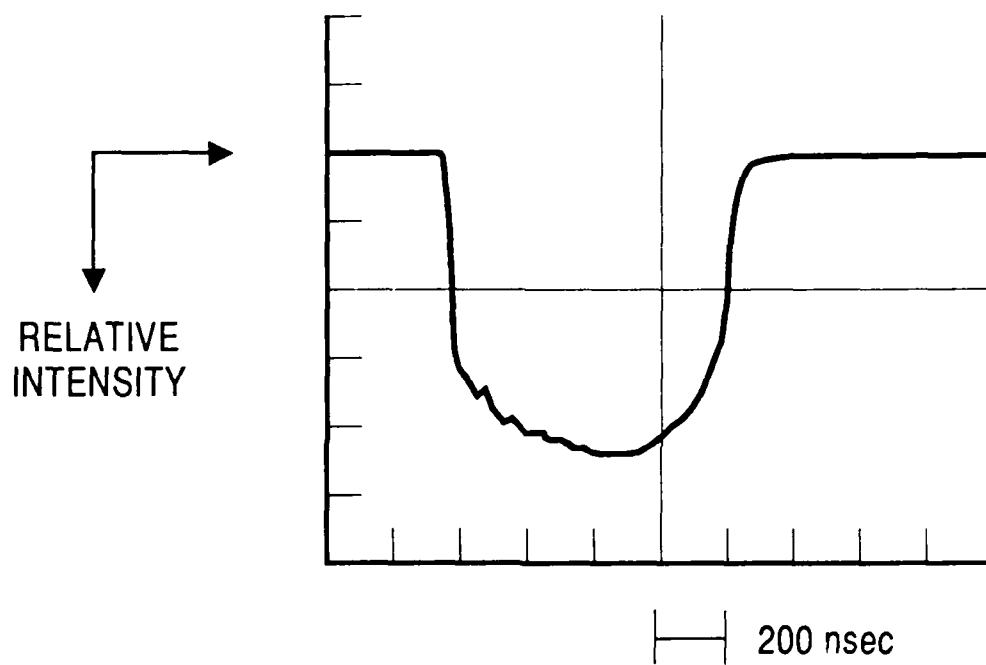


Fig. 3. KrF Laser Output.

D. ULTRAVIOLET PHOTON INJECTION

In the early phases of this demonstration experiment, considerable design effort was applied to the problem of transverse versus collinear photoinitiation by the KrF laser.

The advantages of transverse pumping are the relative simplicity of the optical train, the achievable medium uniformity of photolytic products, and the large margin for scalability of absorbing reagents such as NF_2 and TMB. The optical train does require a cylindrical mirror or lens in the system, as shown in the original experimental concept (Fig. 4). A trial with this geometry, using a fused silica tube, demonstrated that the overwhelming disadvantage of the approach was the long fluorescence lifetime of the cell. Since the major objective of this effort was to maintain a strong optical diagnostic capability under all conditions of operation in the chemical medium, the decision was made to use the collinear configuration in these experiments. Collinear in this case means insertion of the KrF laser along an optical axis coincident with the axis of the cylindrical cell.

An advantage of collinear pumping is the more efficient use of the ultraviolet photon flux. A secondary advantage is that the approach is more compatible with transverse flows in the event that a Bi metal source is substituted for TMB. A disadvantage is the increased complexity in optical train elements. For a BiF lasing experiment, dichroic mirrors with high KrF laser transmission (and low absorption) and with very high reflectances at 457 nm must be made. With varying degrees of success, three manufacturers produced three sets of 1-in. mirrors with around 80% KrF laser transmission and better than 0.99 reflectance at 457 nm. The second complexity is the addition of scrapers for dividing and shaping the KrF beam. We were able to demonstrate that, with a collimated KrF beam, these complexities become relatively minor. A second major disadvantage can be a limitation on NF_2 scaling and medium nonuniformity caused by the greatly increased optical depths involved.

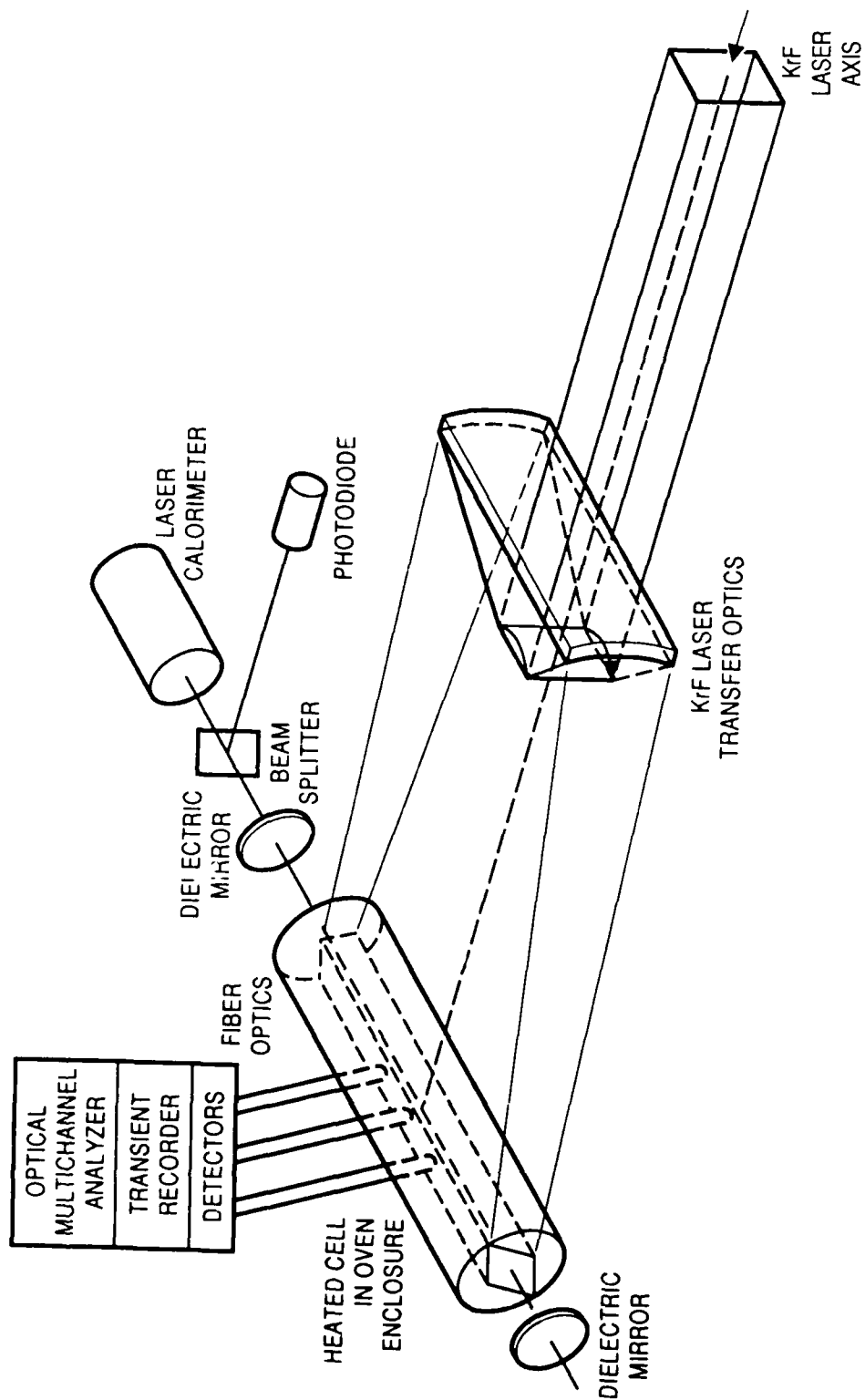


Fig. 4. Schematic of Optical Train for Transverse Laser Photolysis.

Table 3 shows the differences between transverse and collinear pumping for a fixed NF_2 density and fixed laser energy. The nonuniformity can be considerably moderated by using equal counterpropagating pump beams, in which case the nonuniformity can be reduced to under 5%. Figure 5 shows such a geometry.

E. OPTICAL CALIBRATIONS

Two types of optical calibrations are used to determine the absolute densities of $\text{NF}(a^1\Delta)$ and $\text{BiF}(\text{AO}^+)$. The actinometric method depends on a thorough understanding of the products of photodissociation of NF_2 by KrF laser photolysis. The photomultiplier responsivity is calibrated on the basis of the measured signal for a photolyzed NF_2 mixture and the $\text{NF}(a^1\Delta)$ density computed for that photolyzed mixture using the previously measured quantum yield of $\text{NF}(a^1\Delta)$ for the photolysis of NF_2 . The rest of the procedure can then be anchored relative to this reference result. The second approach is the traditional absolute intensity calibration method using known reference radiation sources with specified geometries. The reference sources used in the current experiments included a blackbody source, a tungsten ribbon lamp, and an argon ion laser. Careful calibrations are required in the two wavelength regions around 457 and 874 nm.

This enormous effort was undertaken because it was difficult to obtain satisfactory agreement among the observations made by the different approaches. The results of the calibrations are reported in Section III. These data indicate that absolute densities deduced using the actinometric approach are a factor of 5 larger than those measured with an absolute calibration of the photomultiplier. In this section, we discuss the methodologies of the two approaches. In Section III, our best reconciliation of the discrepancies is offered.

Table 3. Comparison of Transverse and Collinear
KrF Laser Pumping^a

	Transverse Double Pass	Collinear Half Tube
NF ₂ density (mol-cm ⁻³)	2.28×10^{-8}	2.28×10^{-8}
Laser energy (J)	10	5 (10 J total)
Tube diameter (cm)	2	2.5
Tube length (cm)	50	50 (half tube = 25)
Useful tube area (cm ²)	100	4.9
Photon flux (No.-sec ⁻¹ -cm ⁻²)	1.79×10^{23}	1.82×10^{24}
Intensity flux (W-cm ⁻²)	143	1457
NF ₂ dissociation (%)	14	53
Total optical depth	0.033	0.21
$\Delta I/I_0$ uniformity	0.03	0.19

^aNF₂ absorption cross section = 6×10^{-19} cm²

Laser pulse duration = 0.7×10^{-6} sec

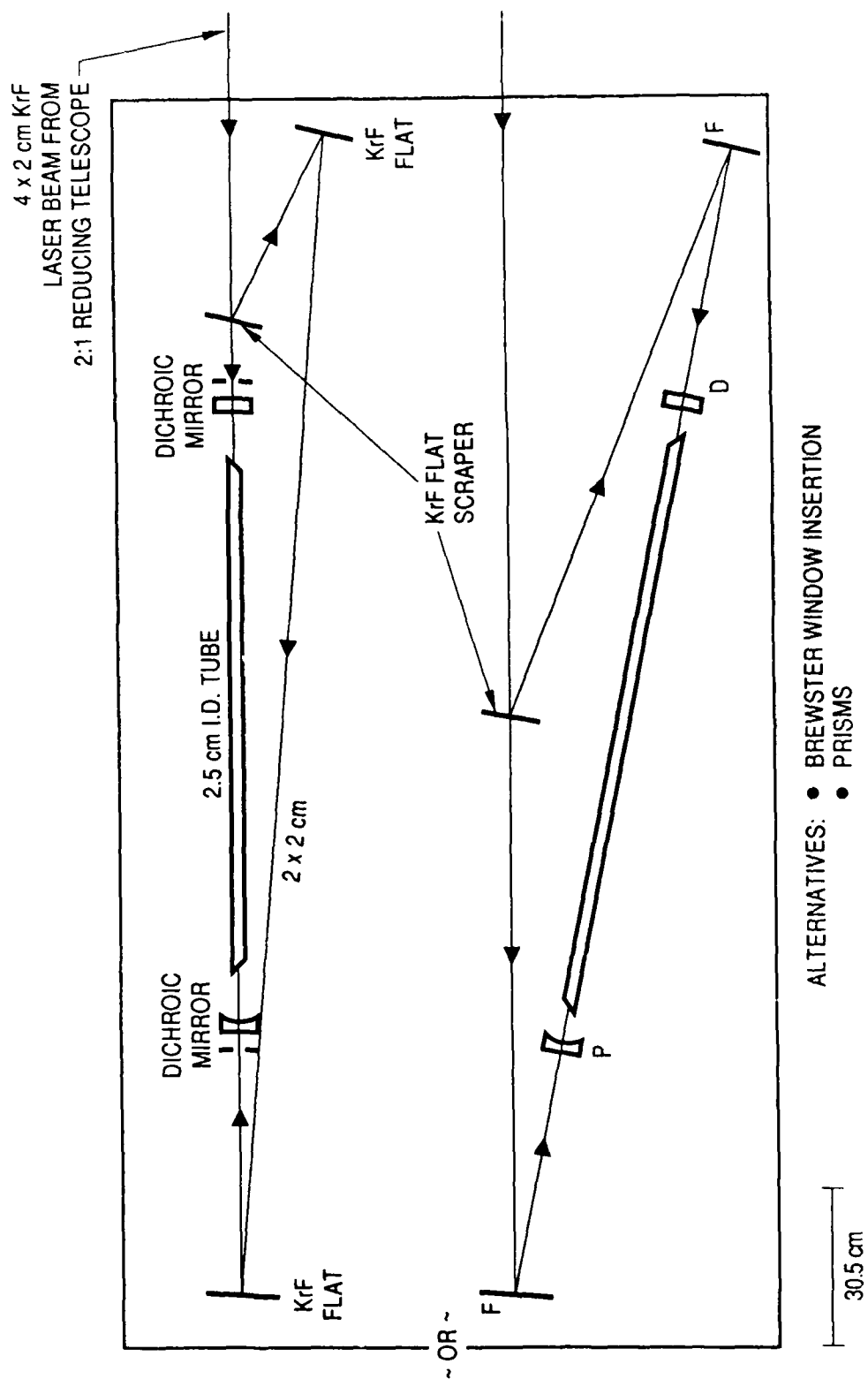


Fig. 5. Schematic of Optical Train for Collinear Laser Photolysis.

1. ACTINOMETRIC APPROACH - NF_2 PHOTODISSOCIATION

Heidner et al.¹³ observed that KrF laser photolysis of NF_2 yields $(10 \pm 5)\%$ $\text{NF}(a^1\Delta)$. This yield was deduced from a kinetic analysis of observed emission traces. If the deduction is correct, the measurement of laser flux, cell temperature, pressure, and N_2F_4 flowrate immediately gives the density of $\text{NF}(a^1\Delta)$ in the system. As noted below, thermal dissociation of N_2F_4 to NF_2 can be verified by an absorption measurement. The advantage of actinometry is that it provides an in situ determination of the $\text{NF}(a^1\Delta)$ density which is valid under any operating conditions so long as the optical train does not change and there are no interfering emissions. Furthermore, only a relative calibration of the detector responses at 874 and 457 nm is required to calibrate absolutely the detection system for 457 nm since the spectroscopy and all other optical component changes such as optical filter factors can be easily calculated or measured. It was difficult, however, to obtain a reference source with really well-defined radiances at both wavelengths. The calibration expression, containing relative ratios of all wavelength dependent factors, is provided in Section III, together with the calibration results.

2. REFERENCE SOURCE APPROACH

The conventional technique for absolute intensity calibrations using standard reference sources is shown in Fig. 6. This calibration cannot be performed in situ because the reference source must be placed in line along the optical axis. The optical train can be approximately duplicated, however. The most uncertain quantities are the detector system solid angle and optical volume. In order to address these issues, traversing pin lamps have been used to define the spatial boundaries of both the calibration setup and the main experiment. The main goal of the calibration is to evaluate detector system responsivity, R , in volt/watt.

Considerable difficulty was experienced with the production of absolute or relative source radiance at the two wavelengths. Commercial black-bodies are designed primarily as infrared radiance standards and are not

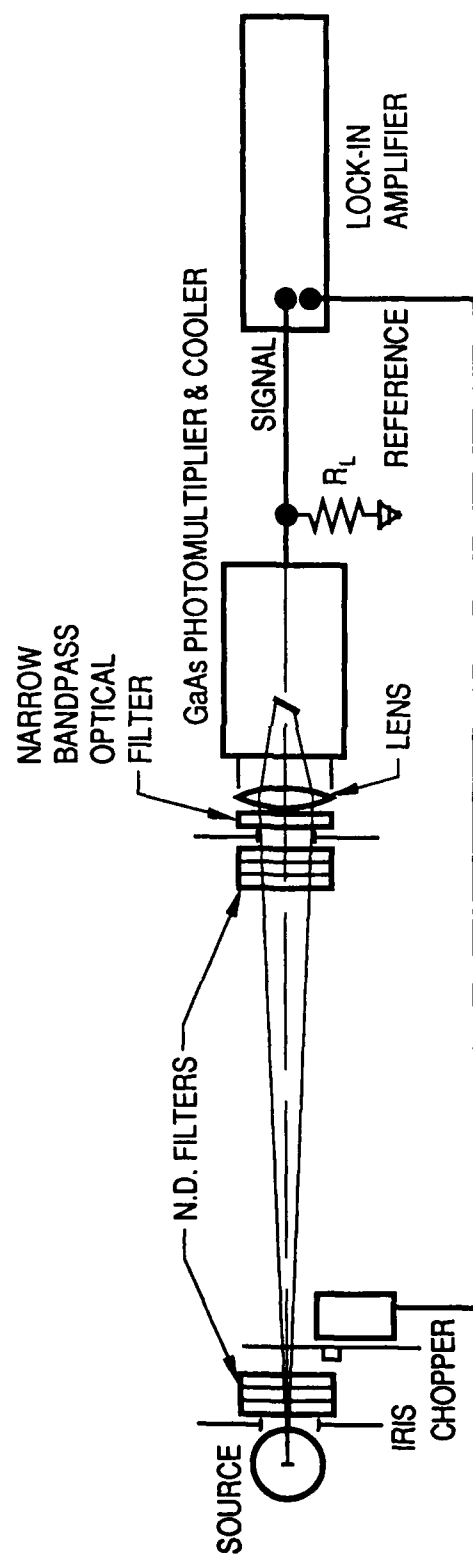


Fig. 6. Calibration Schematic - Reference Approach.

applicable to the blue wavelength. The tungsten ribbon lamp is a better source, but the radiance still increases over two orders of magnitude from blue to infrared. Care must be used in determining the brightness temperature of the tungsten lamp with an optical pyrometer, since a 2°C uncertainty in the temperature leads to a 2% uncertainty in the lamp radiance at 457 nm.

The absolute responsivity at 457 nm obtained with the tungsten lamp calibration was checked with an air-cooled argon ion laser. The laser power can be directly measured with a calibrated power meter. The attenuated argon ion laser beam can then be directed into the photomultiplier detector system, which produces the voltage signal. The attenuators are neutral density filter stacks with accurately determined filter transmissions. The argon ion laser calibration at 465.9 nm agreed with that of the tungsten lamp within 7% at 457 nm, giving some confidence in the absolute calibration. We believe that the tungsten lamp responsivity result at 874 nm should be accurate, because previous calibrations on other systems have shown good agreement between direct tungsten lamp and blackbody radiance sources.

3. ABSORPTION EXPERIMENT FOR NF_2

Figure 7 shows the in situ absorption experiment which yields the degree of thermal dissociation of N_2F_4 under various conditions of cell heating by the oven facility. The ultraviolet radiation source is a highly collimated deuterium lamp. A wide range of N_2F_4 densities can be sampled by tuning the monochromator to different wavelengths in the absorption spectrum of NF_2 . Results in Section III will show that the dissociation is substantial, but not complete. Incomplete dissociation can lead to errors in estimating $\text{NF}(a^1\Delta)$ densities by the photodissociation approach. Dissociation is found to be around 80% for the baseline operating condition.

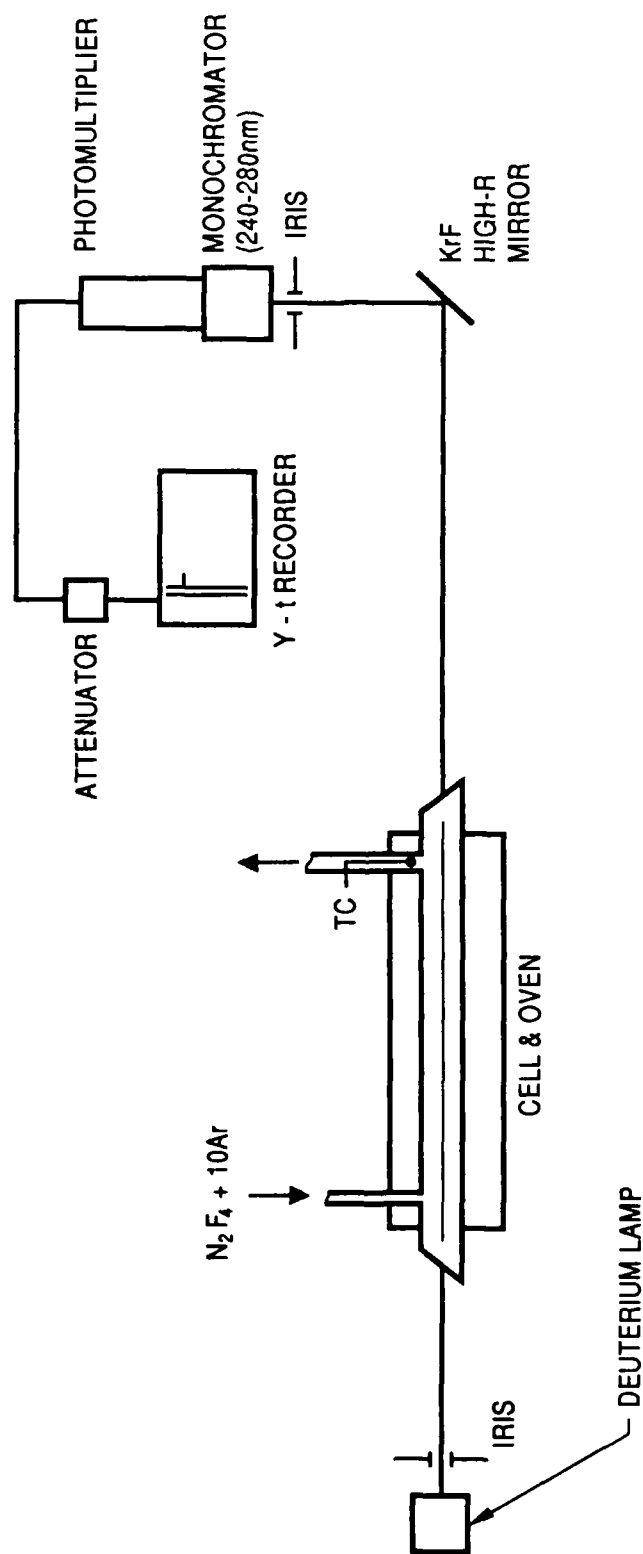


Fig. 7. Absorption by NF_2 .

F. OVEN UNIFORMITY STUDIES

To better understand the thermal dissociation of N_2F_4 , a series of studies were undertaken to assess gas phase thermal uniformity within the cylindrical cell. These measurements were accomplished using axially traversing thermocouples. In addition, a thermocouple rake was used to determine if there were radial temperature variations. We conclude that the oven box must be totally closed for proper thermal uniformity. In principle, this means that sealed window ports (possibly thermopanels) need to be used. For the work reported here, however, sealed ports were not in place. As a consequence, the rectangular slot in the oven for side viewing leads to significant thermal nonuniformities in the middle of the tube. Such temperature variations contribute 10 to 20% errors in the estimate of NF_2 during an experiment.

G. KrF LASER MIRROR EVALUATION AND CELL WINDOW TRANSMISSION

Critical to this experiment is the delivery of KrF photon flux into the cell. Highly efficient transport is dependent on each optical component in the beam train. Since ultraviolet wavelength multilayer dielectric coatings are known to deteriorate under repeated high fluence loadings or during extended exposure in a typical laboratory environment, posttest calibrations of mirror reflectances were conducted as shown in Fig. 8a. Using the technique of testing three mirrors, two-at-a-time, one can determine the absolute 45 deg reflectance of all three (Fig. 8b). Large post-test degradations in reflectance were found.

Transmission of the Brewster windows were measured with the linearly polarized, air-cooled argon ion laser and a power meter in the usual manner. Because the KrF laser is randomly polarized, there are slight losses involved for the Brewster angle configurations. In addition, the downstream window was found to be noticeably clouded.

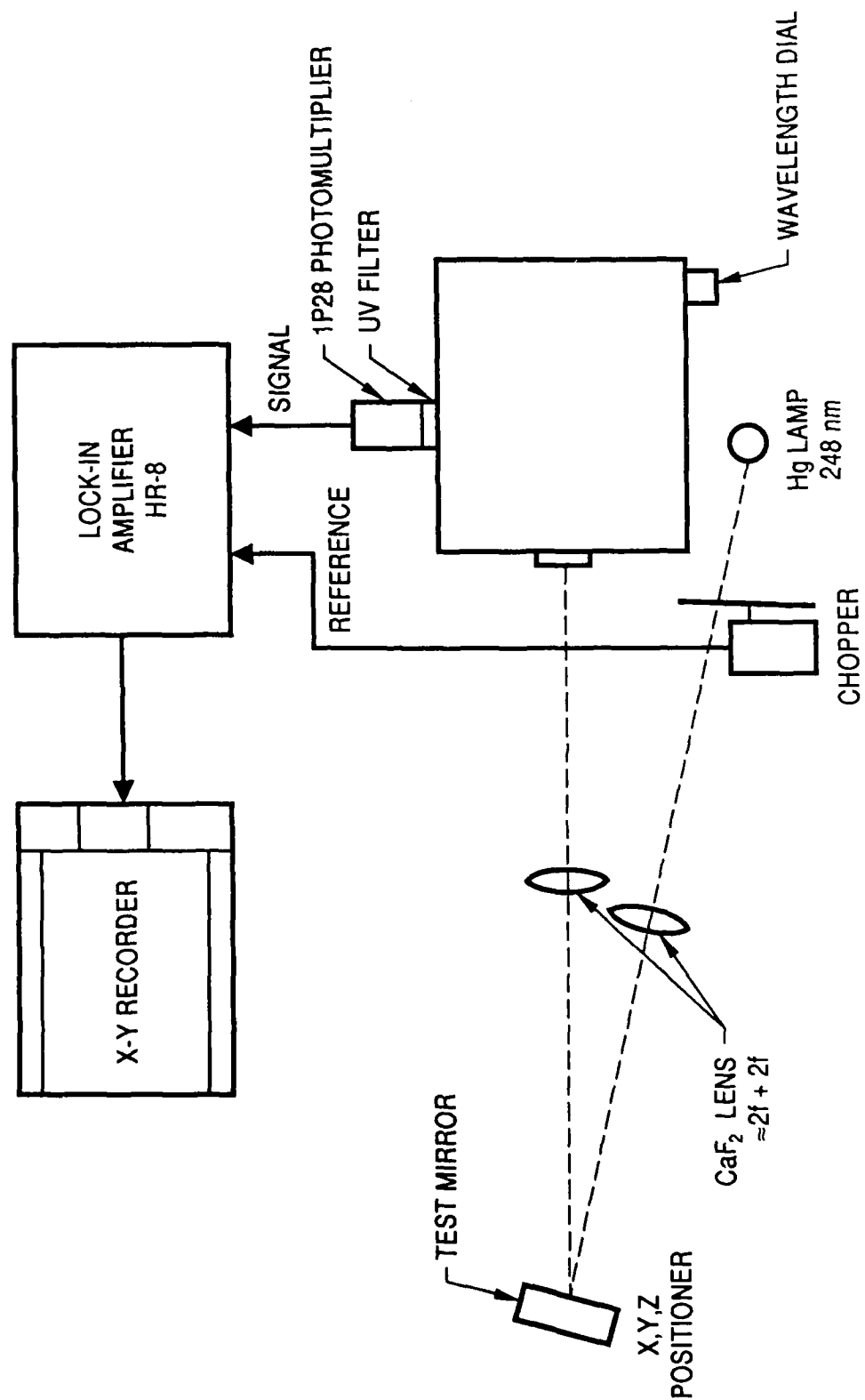


Fig. 8a. Schematic for Laser Mirror Reflectance Measurements.

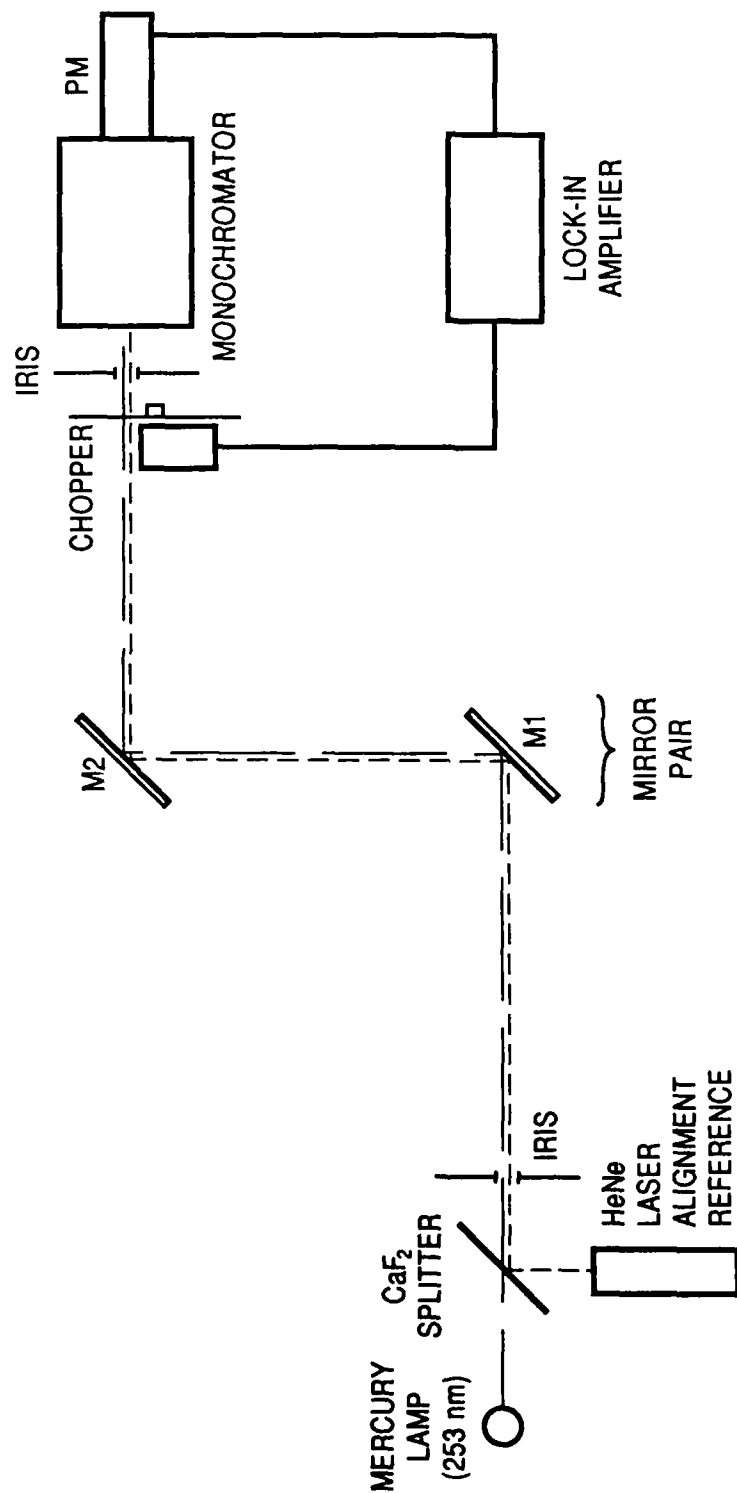


Fig. 8b. Schematic for Absolute Reflectance Measurements.

To summarize, the effective posttest throughput of the upstream leg of the KrF laser beam train was found to be 0.37; throughput of the downstream leg was 0.54 (Fig. 1). Therefore, considerably less flux enters the system than planned, and the photodissociation is somewhat nonuniform over the length of the cell.

III. KINETICS AND SPECTROSCOPY EXPERIMENTS

A. PHOTOMETRIC MEASUREMENTS OF BiF(A,v=0) AND NF(a¹Δ)

As previously discussed (Sections II.E.1 and II.E.2), the maximum density of BiF(A,v=0) generated by the chemical reactions following photo-initiation can be determined by two approaches. The density can be determined from the measured BiF emission at 457 nm on the basis of an absolute calibration of the photomultiplier, the optical geometry, and the spectroscopic parameters of the BiF transition. A second approach is the determination of the BiF density from its emission relative to the NF(a¹Δ) emission from a photolyzed NF₂/argon gas mixture, the computed NF(a¹Δ) density, and the relative spectroscopic parameters. Both of these approaches were used and will be described.

Two sets of baseline experiments were conducted. The full mixture of TMB, H₂, NF₂, argon, and SF₆ diluent, called the "laser mixture," was used in one set of experiments performed to determine the population density of BiF(A) produced at the design conditions. In these "laser mixture" experiments, the BiF(A,v=0) emission was monitored with a photomultiplier through the side of the flow tube, and in some instances, the BiF(A) emission spectrum was recorded with an Optical Multichannel Analyzer (OMA). The second set of baseline experiments was performed to calibrate the photomultiplier with emission from NF(a¹Δ) produced by the photolysis of a gas mixture containing only NF₂/N₂F₄ and argon. A larger load resistor was used, but the photomultiplier was operated at the same voltage so that the emission intensity of NF(a¹Δ) could be compared with the emission intensity of BiF(A) in the "laser mixture" experiments. The NF(a¹Δ) density in these experiments can be computed from the measured KrF laser energy, the NF₂ density, the absorption coefficient of NF₂, and the quantum yield of NF(a¹Δ).

A sample photomultiplier trace of the BiF(A,v = 0) emission from the "laser mixture" is shown in Fig. 9 for Run 1 of November 26, 1986. The fluorescence rose to a peak at about 11.5 μsec after the photolysis laser

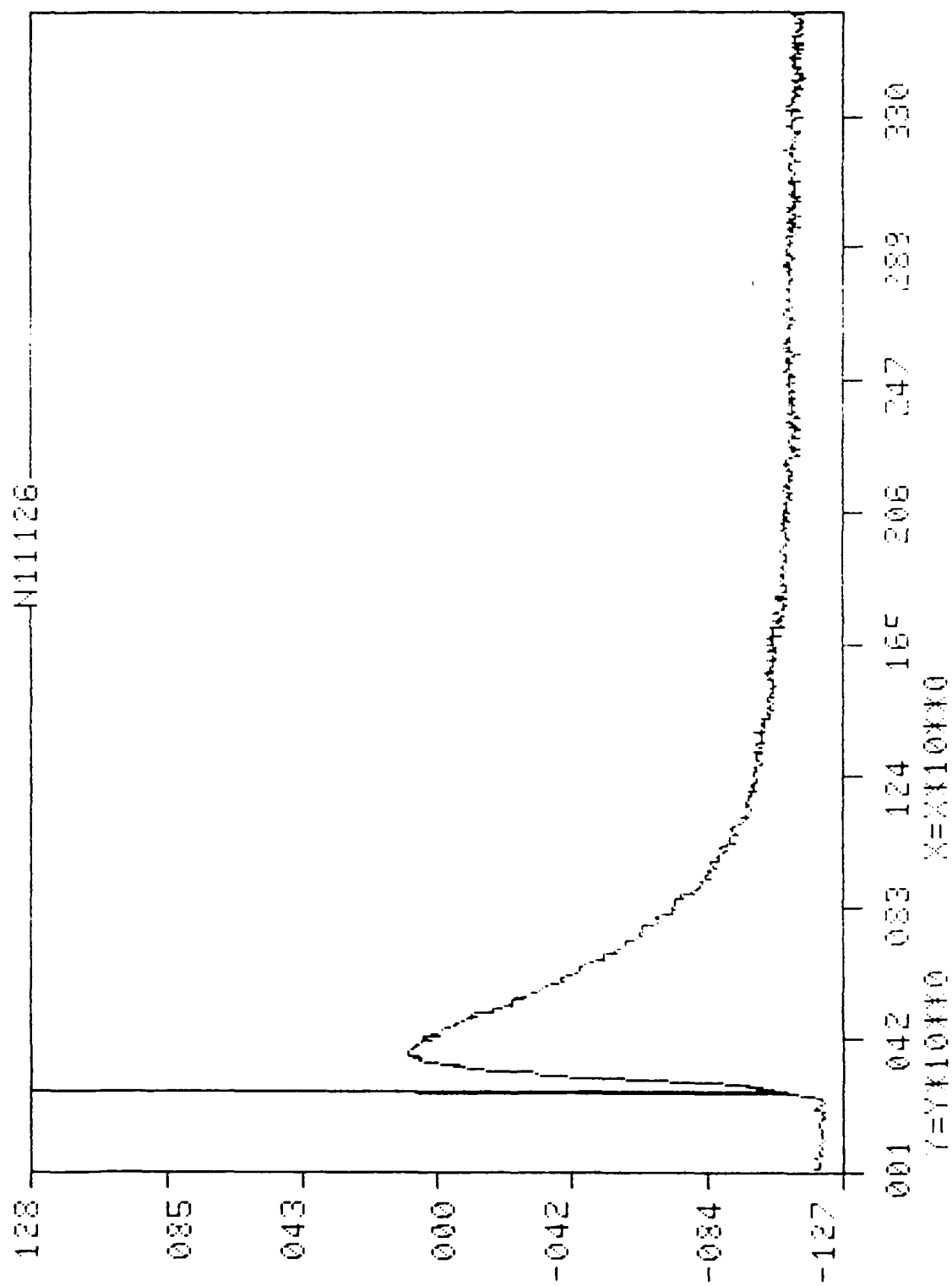


Fig. 9. Photomultiplier Trace of BiF(A) Emission.

pulse and then decayed with an exponential decay time of about 35 μ sec. Very similar traces were recorded in other runs although there was a slight inverse dependence of the peak intensity on the photolysis laser power. The gas composition, laser flux, and the other experimental conditions for this run are listed in Table 1. The gas composition prior to the laser photolysis was calculated from the flow meter readings, the total pressure, and the thermocouple temperature measured at the exit of the flow tube. We assumed that the N_2F_4 was dissociated to NF_2 at an equilibrium concentration determined by the measured temperature.

A sample photomultiplier trace of the $NF(a^1\Delta)$ emission from the NF_2/N_2F_4 and argon gas mixture is shown in Fig. 10 for Run 3 of November 21, 1986. The $NF(a^1\Delta)$ fluorescence rose to a peak at about 50 μ sec after the photolysis laser pulse and then decayed with a decay time of about 1800 μ sec. The $NF(a^1\Delta)$ emission was much weaker than the $BiF(A, v = 0)$ emission from the "laser mixture" in the first set of experiments so that its signal had a lower signal/noise ratio. The gas composition, laser flux, and other experimental conditions for the $NF(a^1\Delta)$ calibration run are also listed in Table 1.

We will first describe the BiF density determination based on the absolute calibration. As described in a previous section, the photomultiplier was calibrated with a tungsten lamp at 457 nm and also with a CW argon ion laser at 466 nm. These two calibrations agree within 7% giving us some confidence in the accuracy of the absolute calibration. The measured photomultiplier voltage is related to the $BiF(A, v = 0)$ density by the equation:

$$\text{Volts} = \text{Res} \times \text{GAIN} \times (h\nu/4\pi) \times A_{ul} \times SR \times A \times L \times Q \times \eta \times FM \times FF \times ND \times [BIF(A, v=0)] \quad (10)$$

The parameters for this equation are listed and defined in Table 4. The volume ($A \times L$) in the equation is determined by the size of the photocathode, the magnification of the optics, and the diameter of the flow tube. The solid angle is defined by the aperture and its distance from the

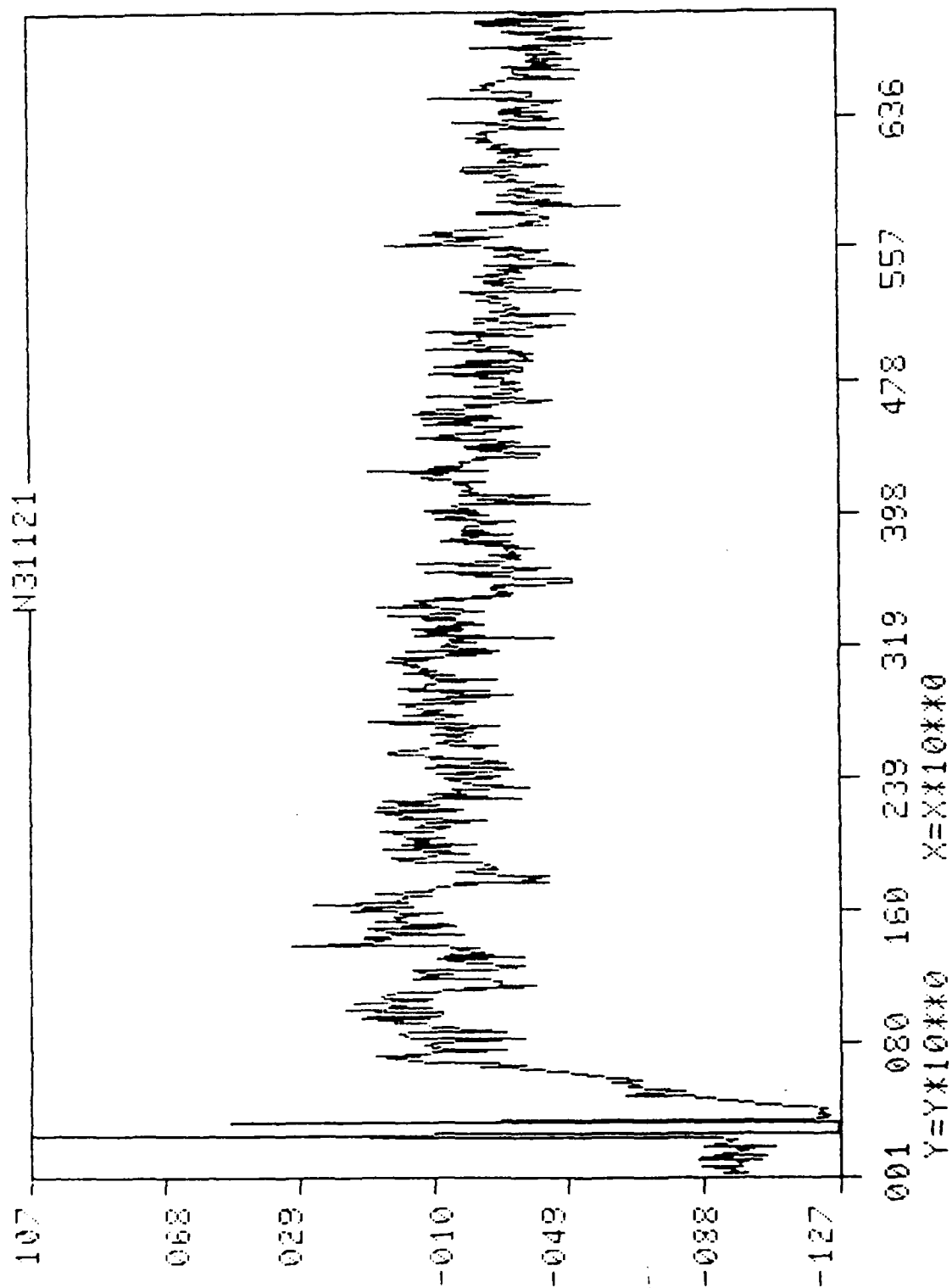


Fig. 10. $NF(a^1\Delta)$ Emission from the N_2F_4 /Argon Mixture.

Table 4. BiF (A,0) and NF(a¹Δ) Density Calculations

(BiF(A,0) Density Determined from Absolute Intensities)

Run No. 1 of November 26, 1986

h	=	6.625E-34	J-sec
ν	=	6.556E+14	1/sec
A	=	9.92	cm ² , effective projected area of photocathode
L	=	2.2	cm, effective diameter of flowtube
SR	=	1.01E-04	steradian
Aul	=	710000	1/sec, inverse lifetime
Q	=	0.2027	Frank Condon factor
η	=	0.8464	flow tube surface losses
FM	=	2.52	light shield and mirror enhancements
FF	=	0.17	interference filter factor
GAIN	=	5	amplifier gain
ND	=	0.105	neutral density filter factor
V	=	0.255	signal in volts
RES	=	878600	volts/watt based on the tungsten lamp and 330 ohms

$$[\text{BiF}(A, \nu = 0)] = (V/\text{RES}) \times 4 \times \pi / (h \times \nu \times A \times L \times \text{SR} \times \text{Aul} \times Q \times \eta \times \text{FM} \times \text{FF} \times \text{GAIN} \times \text{ND})$$

$$[\text{BiF}(A, \nu = 0)] = 1.39 \times 10^{11} \text{ molecules/cc}$$

(NF(a¹Δ) Density Determined from Absolute Intensities)

Run No. 3 of November 21, 1986

h	=	6.625E-34	J-sec
ν	=	3.425E+14	1/sec
A	=	9.92	cm ² , effective projected area of photocathode
L	=	2.2	cm ² , effective diameter of flowtube
SR	=	4.89E-04	steradians
Aul	=	0.172	1/sec, inverse lifetime
Q	=	0.96	Frank Condon factor
η	=	0.8464	flow tube surface losses
FM	=	2.52	light shield and mirror enhancements
FF	=	0.262	interference filter factor
GAIN	=	50	amplifier gain
ND	=	1	neutral density filter factor
V	=	0.187	signal in volts
RES	=	3732273	volts/watt based on the tungsten lamp and 10350 ohms

$$[\text{NF}(a^1\Delta)] = (V/\text{RES}) \times 4 \times \pi / (h \times \nu \times A \times L \times \text{SR} \times \text{Aul} \times Q \times \eta \times \text{FM} \times \text{FF} \times \text{GAIN} \times \text{ND})$$

$$[\text{NF}(a^1\Delta)] = 5.6 \times 10^{13} \text{ molecules/cc}$$

center of the flow tube. The equation includes flow tube suprasil transmission losses of 0.92×0.92 and a back mirror reflective enhancement of a factor of 1.4. It was found that reflections in the light shield between the aperture and the flow tube enhanced the effective solid angle by a factor of 1.8. An effective transmission of 0.17 was calculated for the narrowband interference filter factoring in its actual transmission profile with the spectrum of the BiF(A,0) emission calculated for a temperature of 600 K. A neutral density filter factor, an amplifier gain, the Frank Condon factor for the transition, and the inverse lifetime of the upper state are also included. Using Equation (10) and the photomultiplier voltage from Fig. 9, we calculated a peak BiF(A,v = 0) density of 1.4×10^{11} molecules/cc with the calibration based on the tungsten lamp and a density of 1.5×10^{11} molecules/cc with the calibration based on the argon ion laser. These values are listed in Table 5.

Time-resolved spectra of the BiF(A) emission were taken using a PAR/EGG Optical Multichannel Analyzer (OMAIII) mounted on a McPherson 3/4 meter monochromator. The spectral slit width of 50 μm resulted in a resolution of 0.16 nm. Two movable aluminum-coated mirrors permitted us to obtain OMA spectra of the BiF(A) emission either from the side of the cell or from the end of the cell. The OMA was calibrated for absolute responsivity with the argon ion laser at the same time the photomultiplier was calibrated. A series of measurements of the BiF(A) emission from the laser mixture were performed with different delay times and a 10 μsec gate width. The maximum BiF(A,v = 0) density computed from these measurements was 0.8×10^{11} molecules/cc, which is significantly smaller than the value of 1.5×10^{11} molecules/cc determined with the photomultiplier and the argon ion laser calibration. This measurement may have been affected by the difficulty of collecting emission from the long flowtube through its small diameter or by nonuniformities along the line of sight.

Table 5. $\text{NF}(a^1\Delta)$ and $\text{BiF}(A,0)$ Determinations

"Laser" Mixture $\text{BiF}(A,0)$	Calibration Mixture $\text{NF}(a^1\Delta)$	Method of Determination
1.4×10^{11}	5.6×10^{13}	Absolute calibration - tungsten
1.5×10^{11}	6.0×10^{13}	Absolute calibration - Ar+ laser for BiF plus tungsten relative calibration for $\text{NF}(a^1\Delta)$
7.0×10^{11}	2.8×10^{14}	$\text{NF}(a^1\Delta)$ computed from laser flux $\text{BiF}(A)$ computed on basis relative to $\text{NF}(a^1\Delta)$
8.0×10^{10}		OMA with Ar+ laser absolute calibration
3.4×10^{12}		Model calculation for 10% yield of bismuth

The density of $\text{NF}(a^1\Delta)$ produced in the NF_2 /argon baseline run was determined from the photomultiplier signal of Fig. 10 and the parameters listed in Table 4. We obtained a density of 5.6×10^{13} molecules/cc using the tungsten lamp calibration at 874.2 nm. The tungsten lamp was the only light source available for absolute calibrations at 874 nm. According to the tungsten lamp calibrations, the photomultiplier is less sensitive at the $\text{NF}(a^1\Delta)$ wavelength than it is at the BiF wavelength by a factor of 0.135. These calibrations were performed at the cooled operating conditions of the photomultiplier. The ratio of the red sensitivity to the blue was higher when the photomultiplier was uncooled.

The density of the $\text{NF}(a^1\Delta)$ in the NF_2 /argon baseline run can also be computed from the photolysis laser flux, the NF_2 partial pressure, the NF_2 absorption coefficient, and the quantum yield of $\text{NF}(a^1\Delta)$ at 248 nm. The KrF laser flux is measured with a calorimeter and a splitter plate near the

exit of the laser. However, it subsequently reflects from two specially coated mirrors before entering the flowtube through Brewster's angle windows. Prior to the demonstration experiments, the reflectivity of the mirrors was measured to be better than 98%, and total losses through the optical train were estimated to be about 24% (transmission = 0.76). The Brewster's angle window accounts for most of this loss since the KrF laser is essentially unpolarized. Although the Brewster's angle windows pass one polarization of the laser very efficiently, the other polarization is attenuated by a factor of 0.567. However, measurements performed after the experiments indicated that the mirrors had degraded to a net reflectivity of 0.53 in the upstream leg and 0.88 in the downstream leg. (The downstream portion of the flowtube contained the exhaust port to the pump.) The transmission of the windows had also decreased by factors of 0.89 and 0.78 for the upstream and downstream windows, respectively. Therefore, the postexperiment throughputs were 0.37 and 0.54 for the upstream and downstream legs of the optical train compared with the initial transmissions of 0.76.

The photolysis laser flux at the position in the tube being monitored by the photomultiplier can be estimated by using Beer's law, the NF_2 partial pressure, and the distances from the two ends since the laser is injected from both ends of the tube and is attenuated by the NF_2 . For a laser flux of 0.45 J/cm^2 at the entrance to the optical train, the total flux in front of the photomultiplier is calculated to be 0.37 J/cm^2 for the initial transmission parameters and 0.22 J/cm^2 for the postexperiment transmission parameters. Using an absorption cross section¹³ of $6.8 \times 10^{-19} \text{ cm}^2$, a 7% quantum yield,¹⁴ and an NF_2 density of 2.2×10^{16} , we calculate an $\text{NF}(a^1\Delta)$ density of 2.6×10^{14} molecules/cc for the smaller flux of 0.22 J/cm^2 . It should be noted that this assumes that one absorbed photon dissociates one NF_2 molecule with 7% of the resulting NF being $\text{NF}(a^1\Delta)$. The 7% quantum yield is based on recent work¹⁴ that refines an earlier measurement¹² of $(10 \pm 5)\%$. Bott reanalyzed the earlier measurements and reported¹⁵ a value of $8 \pm 2\%$. The laser is attenuated by the NF_2

absorption by a factor of 0.57 in the upstream leg and a factor of 0.51 in the downstream leg (the optical path is slightly shorter in the upstream portion of the flowtube than in the downstream portion). With a more exact calculation that takes into account the decrease in the NF_2 density during the laser pulse, we obtain an $\text{NF}(a^1\Delta)$ density of 2.8×10^{14} molecules/cc.

This calculated density is larger by a factor of 5.0 than the value of 5.6×10^{13} molecules/cc computed from the measured $\text{NF}(a^1\Delta)$ fluorescence and the absolute photomultiplier calibration obtained with the tungsten lamp. However, if this density of 2.8×10^{14} is believed, we can proceed to compute the $\text{BiF}(A, v = 0)$ density from the relative photomultiplier signals, the relative photomultiplier calibration at the two wavelengths, and the spectroscopic data for the BiF and NF transitions. The pertinent data for this computation are listed in Table 6. We used a lifetime of 5.6 sec for the $\text{NF}(a^1\Delta)$ and 1.4 μsec for the $\text{BiF}(A)$. Another important factor is the photomultiplier responsivity at the wavelength of the NF emission relative to its responsivity at the BiF wavelength. As mentioned previously, the relative response was determined to be 0.135 with the tungsten lamp calibration. Using the parameters of Table 6 we calculate a $\text{BiF}(A, v = 0)$ density of 7.0×10^{11} molecules/cc. Since the value of the $\text{BiF}(A, 0)$ density obtained by this method depends directly on the $\text{NF}(a^1\Delta)$ density, both the $\text{BiF}(A)$ and $\text{NF}(a^1\Delta)$ densities are larger by the same factor of 5.0 than the values calculated on the basis of the tungsten lamp absolute calibrations.

B. NF_2 ABSORPTION MEASUREMENTS

As a check on the actual NF_2 densities in the flowtube, we measured the temperature profile of the heated portion of the tube and performed NF_2 absorption measurements. Temperature measurements with a thermocouple probe along the centerline of the tube indicated the high-temperature portion to be approximately 84 cm long with the temperature dropping off near the gas inlet and gas exhaust. There was also a temperature dip in the middle portion of the tube where an opening in the insulated box

Table 6. Parameters for Measurement of BiF(A) Relative to NF(a¹Δ)

Date	November 21, 1986	November 26, 1986
Run No.	N31121	N11126
Molecule	NF(a ¹ Δ)	BiF(A, v=0)
Density	2.8 × 10 ¹⁴	
Signal(volts)	0.187	0.255
Aul(1/sec)	0.172	710000
q(v'v'')	0.96	0.2027
Rl(ohms)	10350	330
Gain	50	5
N.B. filter	0.262	0.17
ND filter	1	0.105
Iris dia.(cm)	0.66	0.3
Relative response	0.1354	1
Wavelength, Å	8742	4568
v, sec ⁻¹	3.43 × 10 ¹⁴	6.57 × 10 ¹⁴

$$[\text{BiF(A,0)}] =$$

$$\frac{[\text{NF(a}^1\Delta)] \times [\text{A} \times \text{q} \times \text{Rl} \times \text{G} \times \text{NBF} \times \text{ND} \times \text{RelRes} \times \text{v} \times \text{ID}^2 \text{ of NF(a}^1\Delta)] \times [\text{Signal of BiF(A)}]}{[\text{A} \times \text{q} \times \text{Rl} \times \text{G} \times \text{NBF} \times \text{ND} \times \text{RelRes} \times \text{v} \times \text{ID}^2 \text{ of BiF(A)}] \times [\text{Signal of NF(a}^1\Delta)]}$$

$$[\text{BiF(A, v=0)}] = 7.0 \times 10^{11} \text{ molecules/cc}$$

surrounding the tube allowed access for photomultiplier emission measurements. The temperature profile drooped as much as 30°C near the opening in the box but was quite uniform when the opening was covered. The temperature droop was more accentuated when no gases were flowing through the tube. The radiative and convective heat losses through the opening in the heated box wall were larger than we had anticipated.

We determined the NF_2 density by measuring the attenuation of light from a deuterium lamp traversing the length of the flowtube. A monochromator set at 260 nm limited the spectral bandwidth of the detected light to approximately 5 nm. The average NF_2 density was calculated using the absorption coefficient of $1.5 \times 10^{-18} \text{ cm}^2$ measured by Heidner et al.¹³ and the effective flowtube length of 84 cm determined with the temperature probe.

The NF_2 density determined from the absorption measurements for the "laser mixture" was 10% lower than the density calculated from the gas flow rates and the equilibrium constant for the temperature measured at the exit of the flow tube. The discrepancy was somewhat larger (about 15%) for the $\text{NF}_2/\text{N}_2\text{F}_4$ argon gas mixture. Part of this discrepancy may result from the temperature dip in the middle section of the tube where the opening in the box allowed for photomultiplier emission measurements. If the NF_2 density was uniformly 15% lower than the nominal value, then the calculated density of the $\text{NF}(a^1\Delta)$ produced by the photolysis of NF_2 should be lowered by about 6%. The nonlinearity results because lower NF_2 density would allow more of the laser fluence to reach the center of the flowtube. This larger laser fluence partly counterbalances the 15% lower NF_2 so that the $\text{NF}(a^1\Delta)$ is only reduced by 6%. The estimated $\text{NF}(a^1\Delta)$ density would be reduced much more if the NF_2 density is only lowered in the vicinity of the photomultiplier.

C. OMA MEASUREMENTS OF BiF ROTATIONAL AND VIBRATIONAL TEMPERATURES

The effective BiF(A) vibrational (T_{vib}) and rotational (T_{rot}) temperatures were obtained from simulations of the measured spectra using a computer code. This program assumes Boltzmann equilibrium and uses the molecular constants reported by Jones and McLean.¹⁶ The relatively isolated (0,0) band near 437 nm was used to determine T_{rot} . This temperature was varied until the best fit to the data was obtained. T_{rot} was then held fixed, and T_{vib} was then determined from the best fit to the entire OMA spectrum. A total of 16 BiF A - X vibronic bands were used in the simula-

tion. These included the (0,0), (4,3), (2,2), (3,3), (0,1), (1,2), (4,4), (2,3), (3,4), (0,2), (4,5), (1,3), (2,4), (3,5), (0,3), and the (1,4) bands.

A typical simulation of the (0,0) band is depicted in Fig. 11. A rotational temperature of $330 \pm 100^\circ\text{C}$ was obtained. The full OMA spectrum is shown in Fig. 12, from which we obtain $T_{\text{vib}} = 900 \pm 50^\circ\text{C}$. The experimental conditions for Figs. 11 and 12 are as follows: $[\text{NF}_2] = 1.7 \times 10^{16}$ molecules cm^{-3} , $[\text{TMB}] = 5.8 \times 10^{14}$, $[\text{H}_2] = 1.4 \times 10^{16}$, $[\text{Ar}] = 1.0 \times 10^{17}$, and $[\text{SF}_6] = 1.9 \times 10^{17}$. The gas temperature of 147°C was measured with a thermocouple before the reactions were initiated. It should be noted that the spectra in these figures are from the BiF "side light" emission.

In order to determine the time dependence of the $\text{BiF}(\text{A } 0^+)$ state temperature, OMA spectra were recorded at various delays with respect to the KrF laser pulse. Figure 13 indicates two BiF side emission spectra taken at different times. The experimental conditions are the same as those given previously. The two spectra have been normalized for comparison. Since the two spectra are essentially identical, it can be concluded that under these conditions, T_{rot} and T_{vib} are constant for most of the emission duration.

D. OMA MEASUREMENTS OF THE BiF GROUND STATE DENSITY

An estimate of the total BiF ground state density was obtained from the examination of OMA spectra taken down the axis of the photolysis cell. If sufficient $\text{BiF}(\text{XO}^+)$ is present, the $\text{BiF}(\text{A} - \text{X})$ OMA spectra will be "distorted" because of absorption of the spontaneous emission. The BiF spectrum simulation code was modified to account for this absorption. The emission intensity detected by the OMA in this case is given by

$$I(\nu) = \int I(\nu, x) e^{-\sigma(\nu)Nx} dx \quad (11)$$

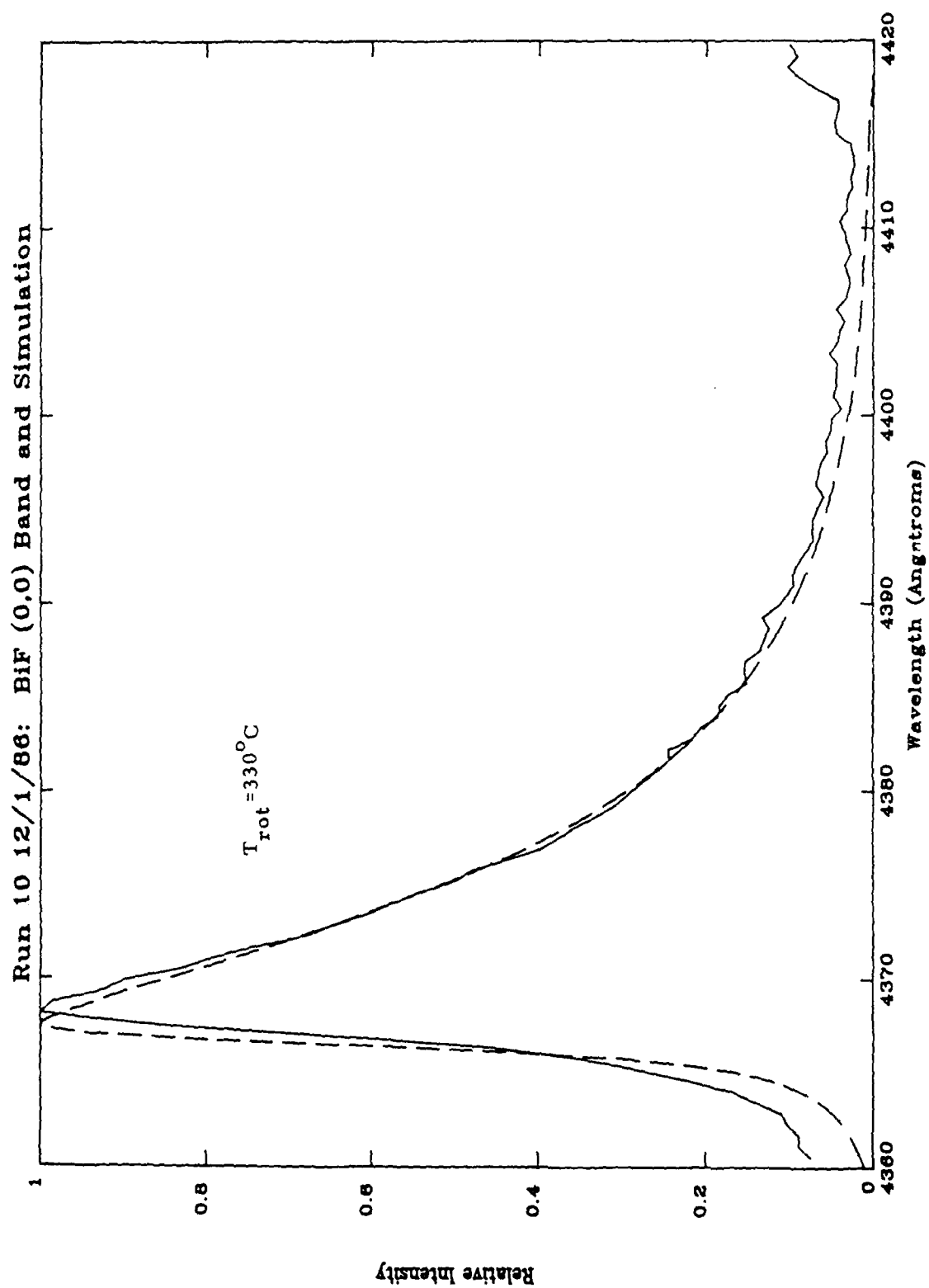


Fig. 11. OMA Measurements and Simulation of the (0,0) Band of BiF(A) for Rotational Temperature Determination.

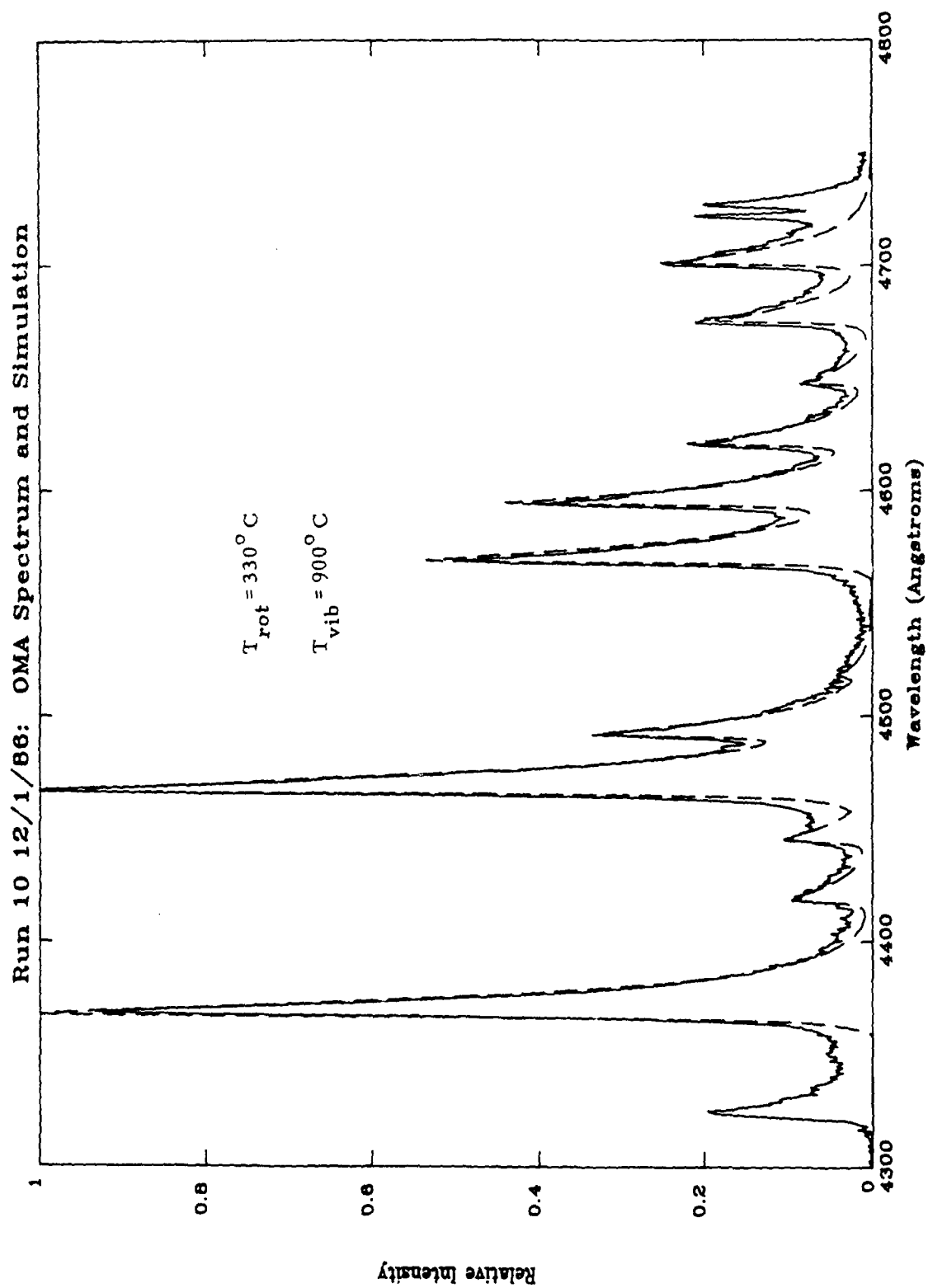


Fig. 12. OMA Spectrum and Simulation of the BiF(A) Emission.

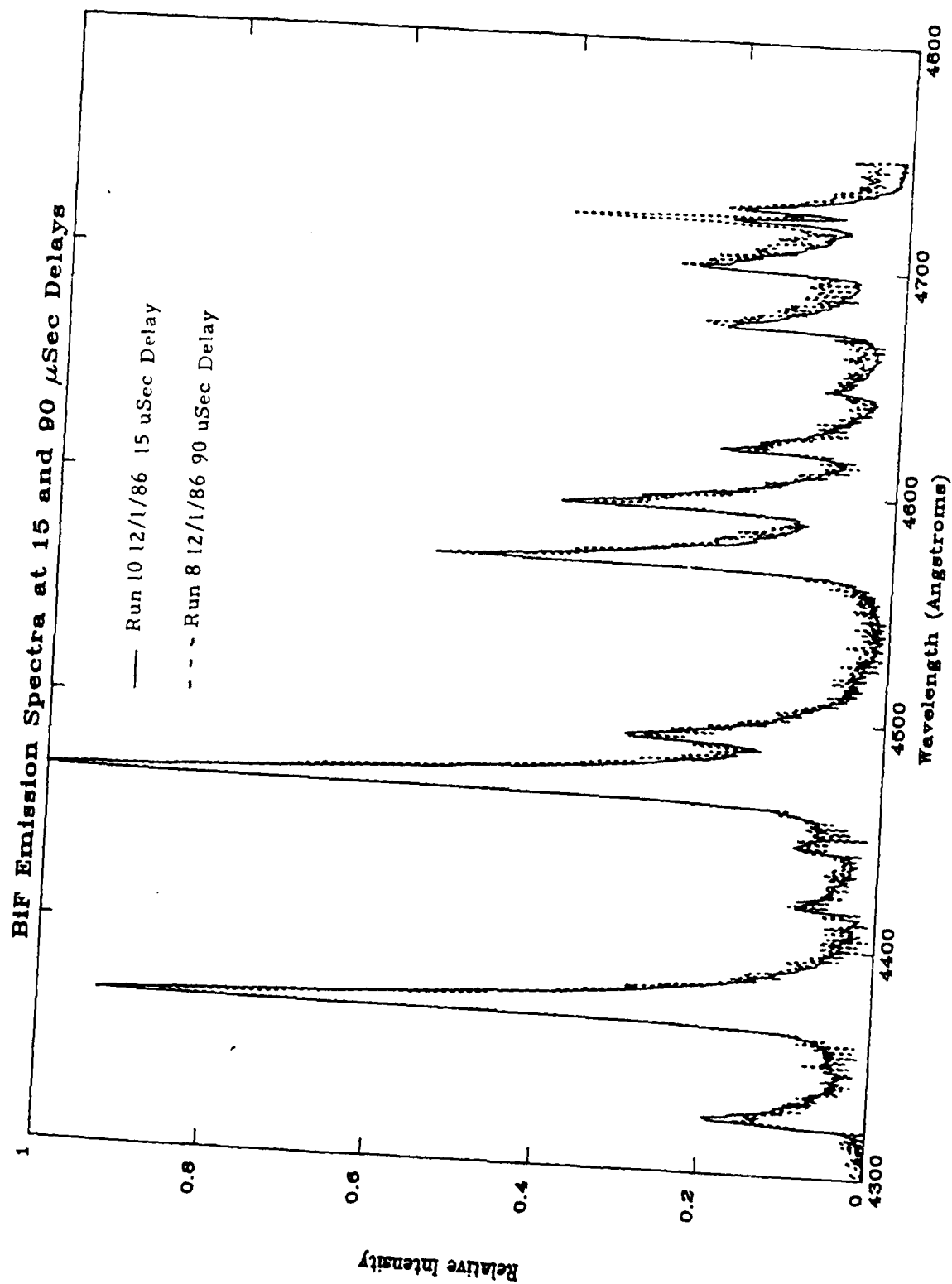


Fig. 13. OMA Emission Spectrum of BiF(A) at Different Delay Times.

where $I(v, x)$ is the emission intensity at position x , $\sigma(v)$ is the absorption cross section, and N is the total BiF ground state density. The evaluation of the integral over our 120 cm cell length gives

$$I(v) = I^0(v) (1 - e^{-\sigma(v)NL})/\sigma(v)N \quad (12)$$

where $I^0(v)$ is the spontaneous emission intensity, and L is the cell length. This equation was incorporated into the simulation code to model the axially viewed OMA spectra. The absorption cross section was taken to be the peak cross section of a Doppler broadened BiF rovibronic line given by:

$$\sigma(v) = (8\pi^3/3ch)(R_e^2 q_{v',v''} S_{J',J''}/(2J'' + 1)) (v/2 \ln(2/\pi))^{1/2} / \Delta v \quad (13)$$

where R_e^2 is the electronic transition moment, $q_{v',v''}$ is the Franck-Condon factor, $S_{J',J''}$ is the Honl-London factor, and Δv is the FWHM Doppler width. From the measured 1.4 μ sec radiative lifetime, we obtain $R_e^2 = 2.03 \times 10^{-1}$ Debye².

An end viewed OMA spectrum is shown in Fig. 14. The best fit to the spectrum was obtained with a total BiF ground state concentration of 5×10^{13} molecules cm⁻³ that is 10% of the initial TMB concentration. The BiF A state T_{rot} and T_{vib} were fixed at their values determined from the side emission, and the ground state T_{rot} and T_{vib} were taken to be 330°C. Figure 15 displays several simulations for different BiF ground state densities to indicate the sensitivity of this procedure, and we estimate that our error for [BiF(X 0⁺)] is on the order of a factor of 2 or 3.

E. EFFECT OF SF₆ SCALING

Several OMA spectra and BiF (0,2) emission traces were recorded where [SF₆] was varied, and densities of the other reagents were held fixed at the values given previously. The BiF(A) state temperatures were determined as described in the previous section. Both T_{rot} and T_{vib} decreased with added SF₆. The results are presented in Table 7. T_{rot} showed a slight

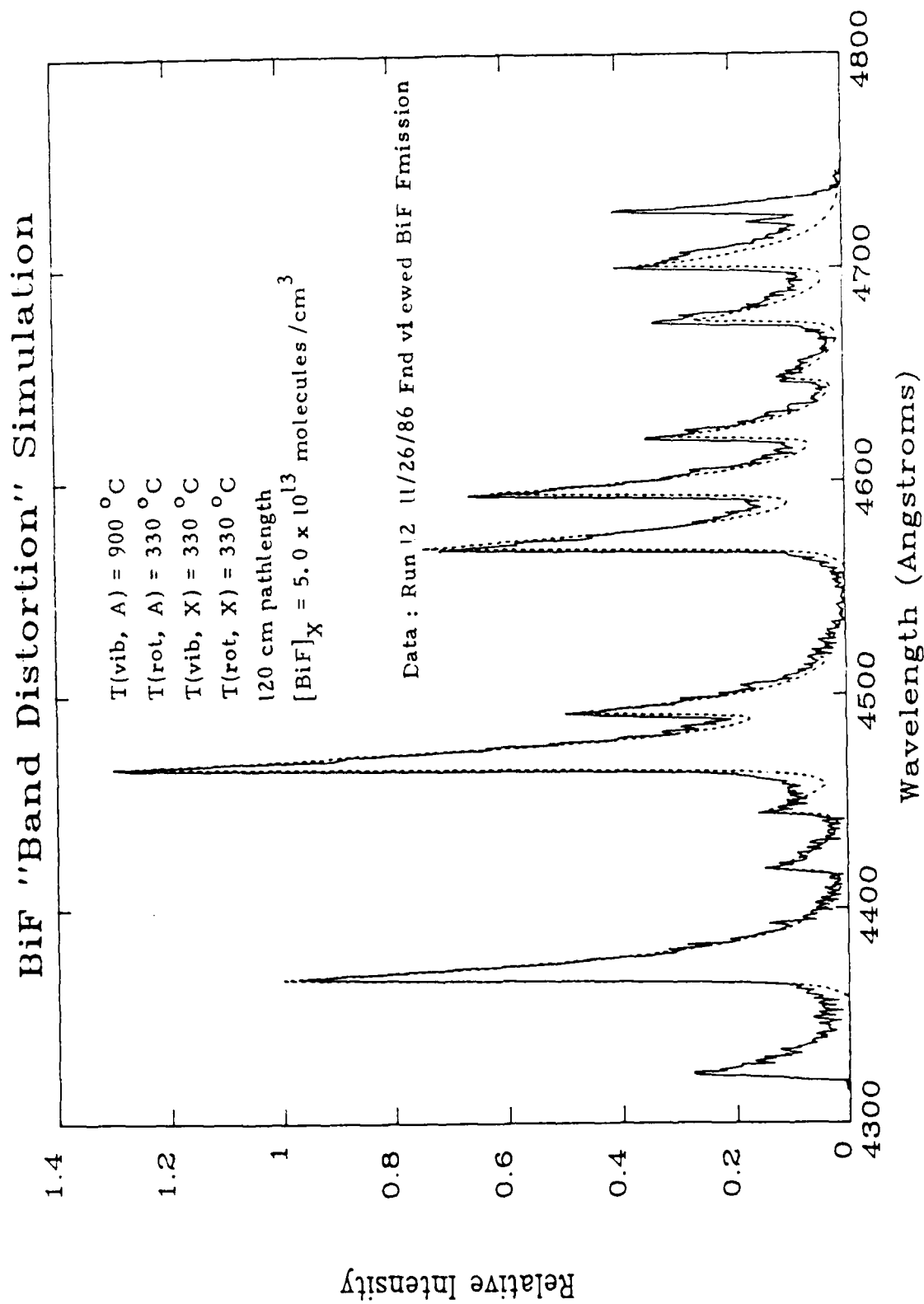


Fig. 14. OMA Measurements of "End-on" BiF(A) Emission and Simulation of the "Band Distortion".

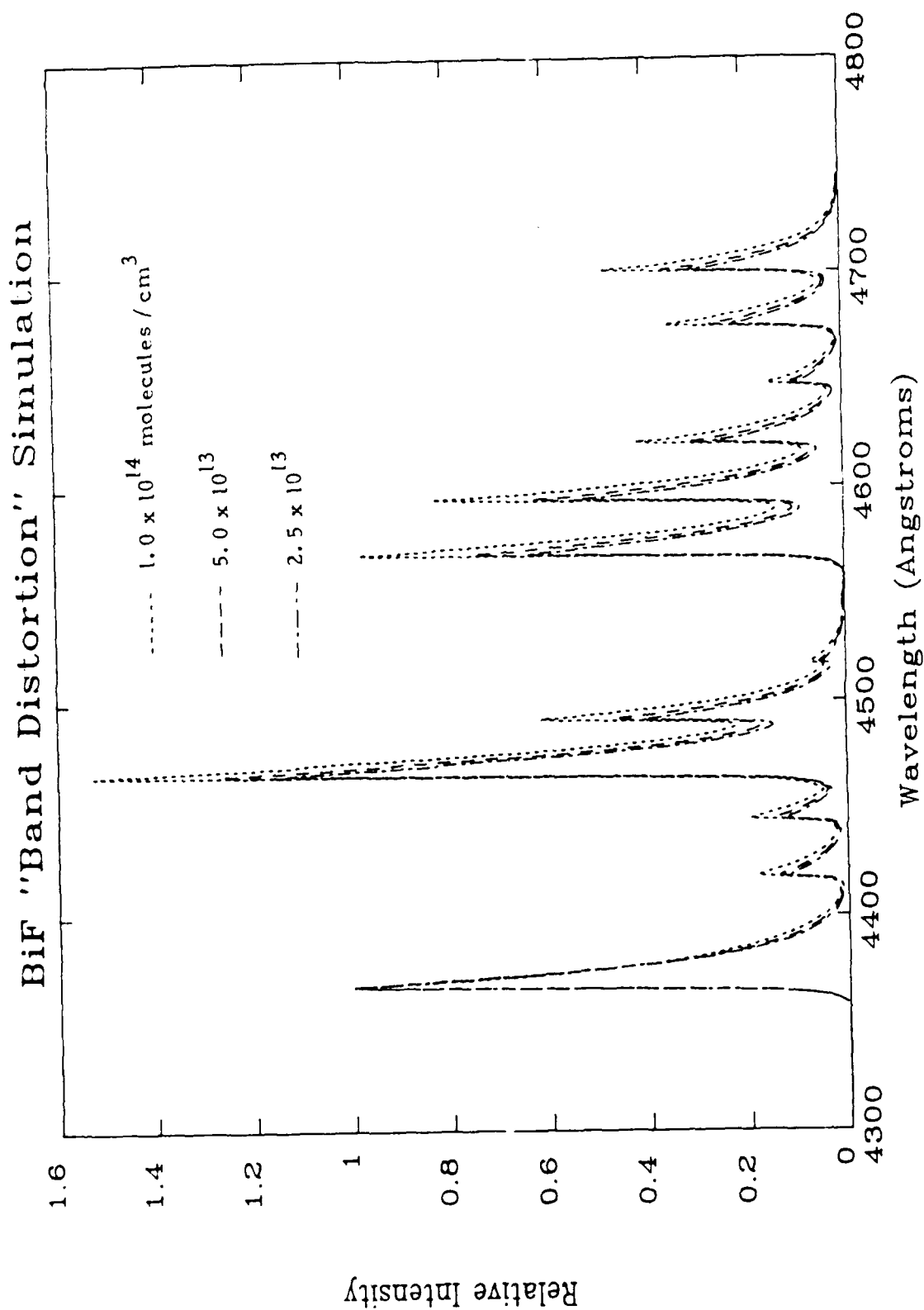


Fig. 15. Sensitivity of BiF(A) Spectrum Simulations for Different Values of BiF(X).

added SF₆. The results are presented in Table 7. T_{rot} showed a slight decrease while T_{vib} decreased from 1200°C at the lowest [SF₆] to 650°C at the highest density. An attempt was made to increase further the SF₆ concentration but spontaneous ignition of the gas mixture occurred under these conditions. Under different reagent densities, ([NF₂] = 1.6 × 10¹⁶, [TMB] = 1.3 × 10¹⁵, [H₂] = 9.2 × 10¹⁵, and [Ar] = 3.7 × 10¹⁷) we were able to obtain stable mixtures with SF₆ densities of up to 1.5 × 10¹⁸. Under these conditions, T_{rot} and T_{vib} dramatically decreased to 250° and 350°C, respectively.

From the knowledge of the BiF A state vibrational temperatures and the BiF (0,2) emission obtained from the GaAs photomultiplier, the behavior of the relative BiF(A) state population as a function of [SF₆] could be determined. The results are listed in Table 8 and presented in Figs. 16 to 19. The density of the BiF v'=0 level increased with added SF₆, reflecting the fact that this level is being populated by relaxation from the higher vibrational levels. In contrast, the total BiF(A) state population is observed to be constant, which is consistent with recent experimental results that quenching by SF₆ is slow.¹⁷

F. EFFECT OF SCALING OF ALL REAGENTS ON BiF A STATE POPULATION

In another set of experiments, the effect on the the BiF A state population of scaling all reagents at fixed stiochiometry was investigated. A mixture that was stable toward ignition was obtained, and then the flow was throttled so that all densities were scaled by the same factor. Time resolved BiF (0,2) emission was recorded, and the results are provided in Table 9. OMA spectra were also taken, and under the small total pressure excursion (8 to 24 Torr), the BiF A state vibrational temperature remained relatively constant. Hence, the data in Table 9 represent the behavior of the total BiF A state population. These data are plotted in Figs. 20 and 21. Both the peak and integrated BiF A state signals depended linearly upon the total pressure. The extrapolated peak signal passes through the origin, whereas the integrated signal does not. This may be caused by a

Table 7. Temperature Variation with Added SF₆

[SF ₆] (molecules cm ⁻³)	T _{rot} (°C)	T _{vib} (°C)
0.79 × 10 ¹⁷	360	1200
1.93 × 10 ¹⁷	330	900
2.88 × 10 ¹⁷	310	750
3.76 × 10 ¹⁷	300	650

Table 8. BiF A State Density with Added SF₆

[SF ₆] molecules cm ⁻³	BiF A v'= 0 Peak	BiF A v'=0 Integrated	BiF A Total Peak	BiF A Total Integrated
0.79 × 10 ¹⁷	120	7600	400	25000
1.93 × 10 ¹⁷	150	8100	400	22000
2.88 × 10 ¹⁷	170	9000	410	22000
3.76 × 10 ¹⁷	190	11000	430	25000

Table 9. BiF A State Density with Total Reagent Scaling

[NF ₂]	[TMB]	[H ₂]	[Ar]	[SF ₆]	BiF A Peak	BiF(A) Inte- grated
1.1 × 10 ¹⁷	4.4 × 10 ¹⁴	5.5 × 10 ¹⁵	6.6 × 10 ¹⁶	1.2 × 10 ¹⁷	115	8200
1.7 × 10 ¹⁶	7.4 × 10 ¹⁴	9.3 × 10 ¹⁵	1.1 × 10 ¹⁷	2.1 × 10 ¹⁷	180	9800
2.7 × 10 ¹⁶	1.2 × 10 ¹⁵	1.5 × 10 ¹⁶	1.9 × 10 ¹⁷	3.4 × 10 ¹⁷	270	12300

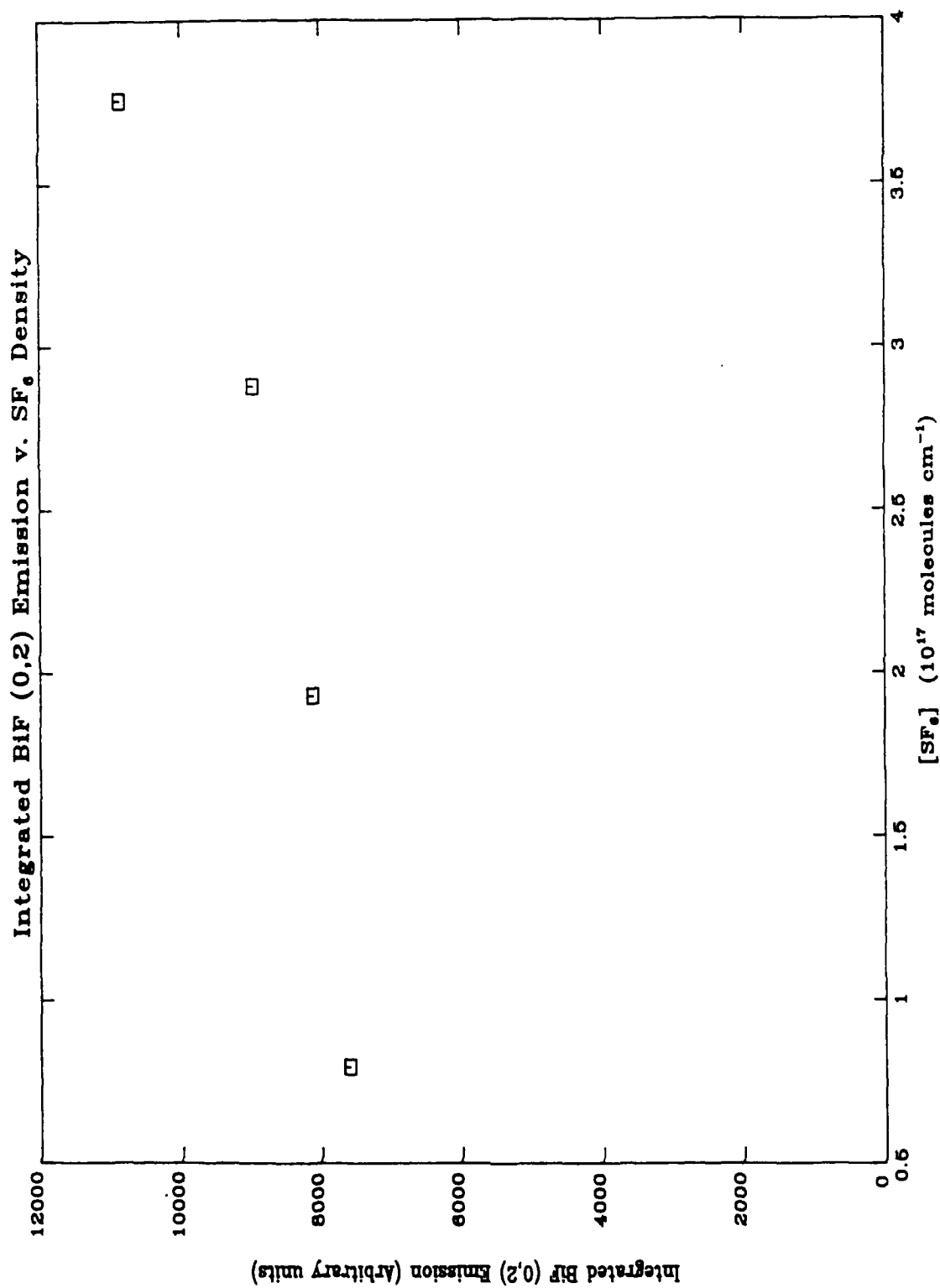


Fig. 16. Integrated BiF(0,2) Emission vs. SF_6 Density.

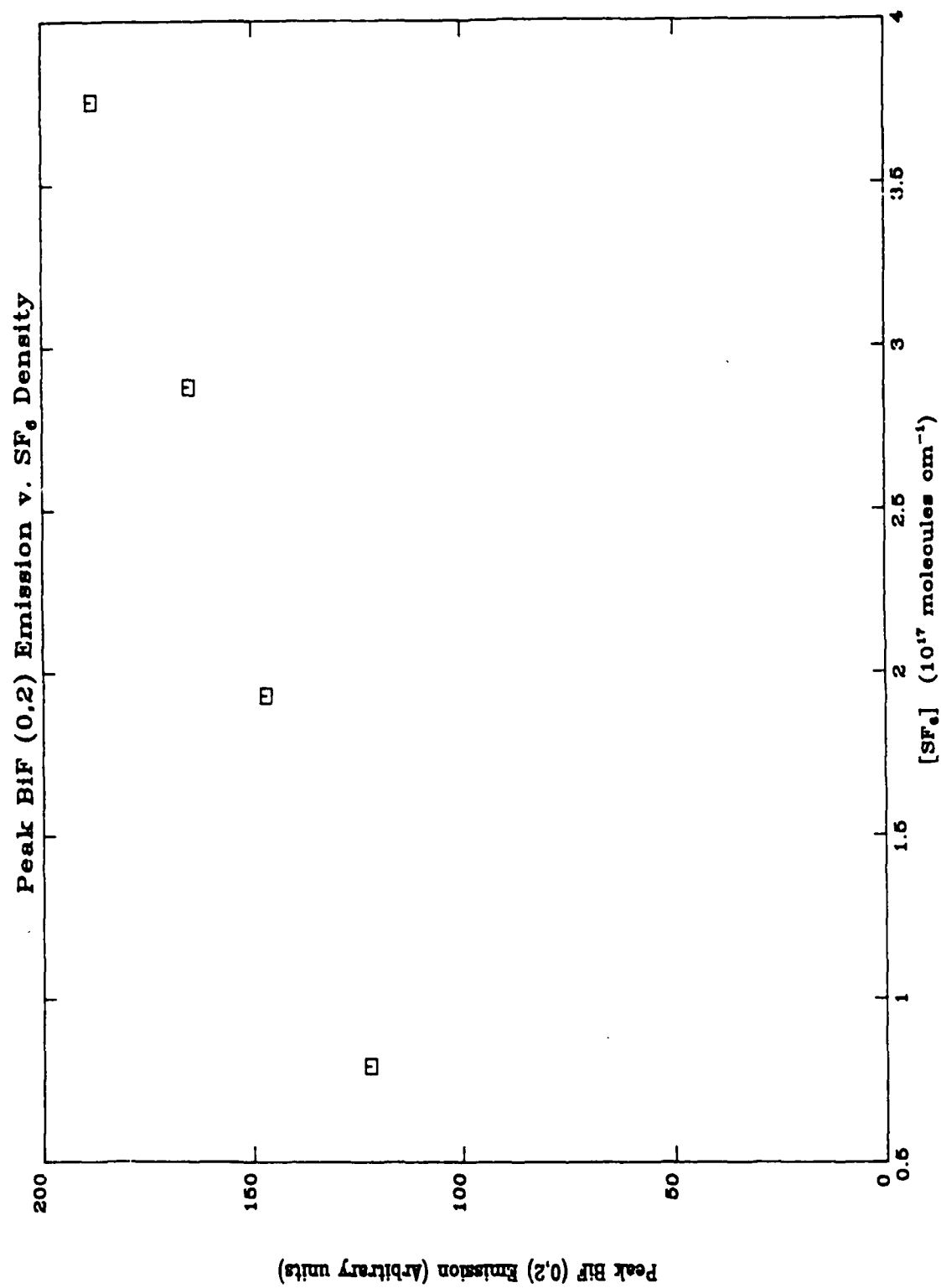


Fig. 17. Peak BiF(0,2) Emission vs. SF₆ Density.

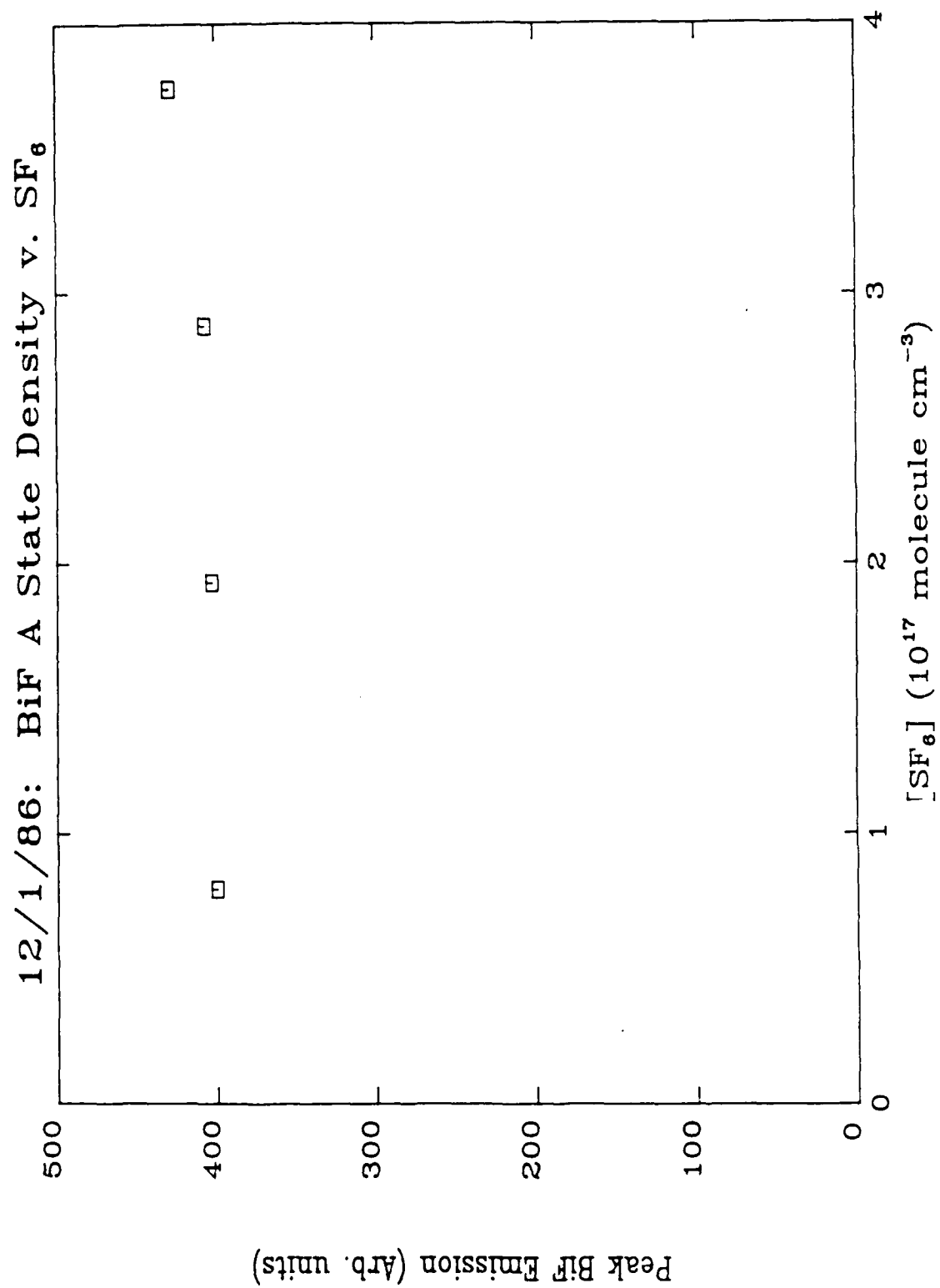


Fig. 18. BiF A State Density (Peak) vs. SF₆.

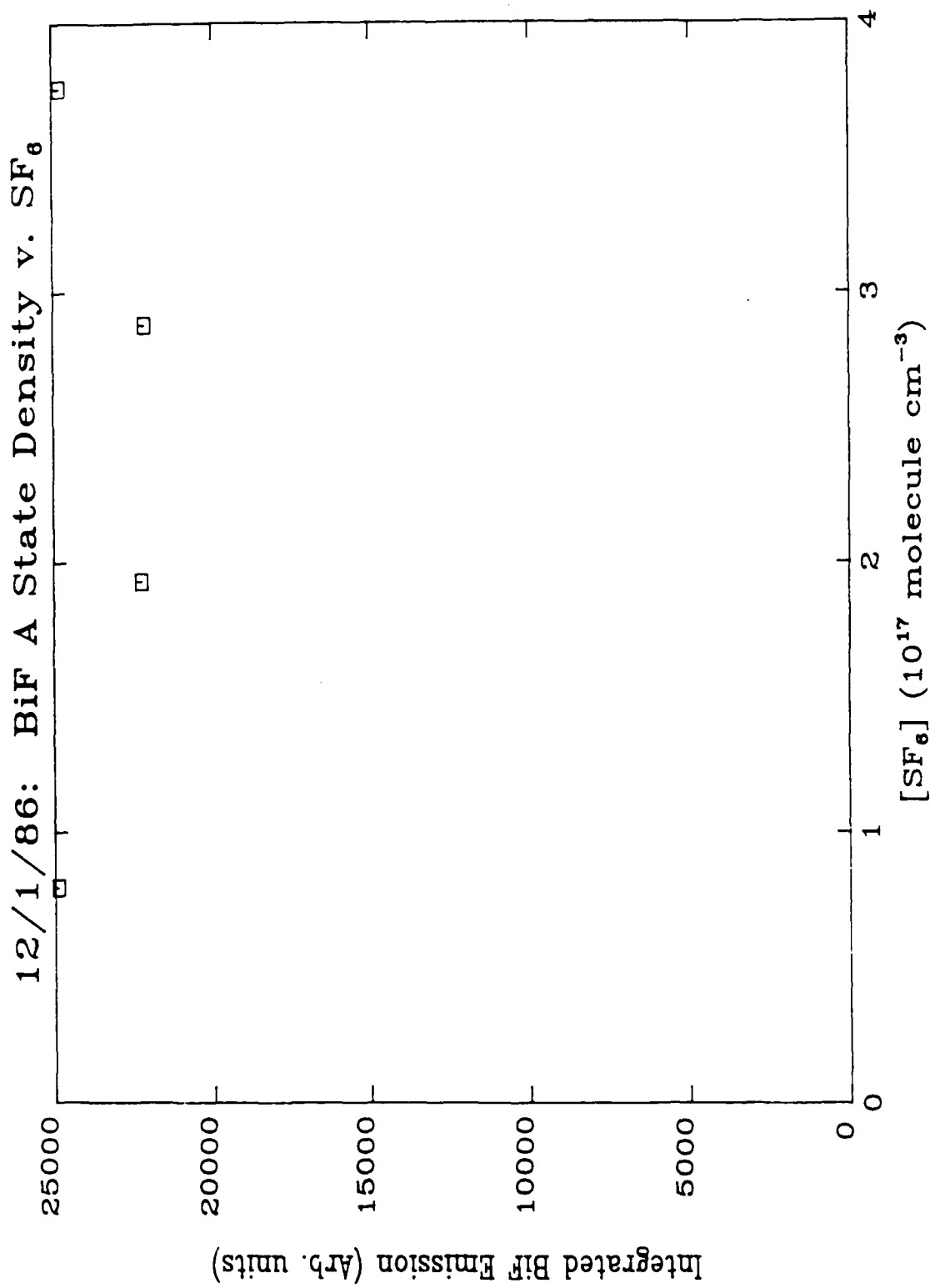


Fig. 19. BiF A State Density (Integrated) vs. SF₆.

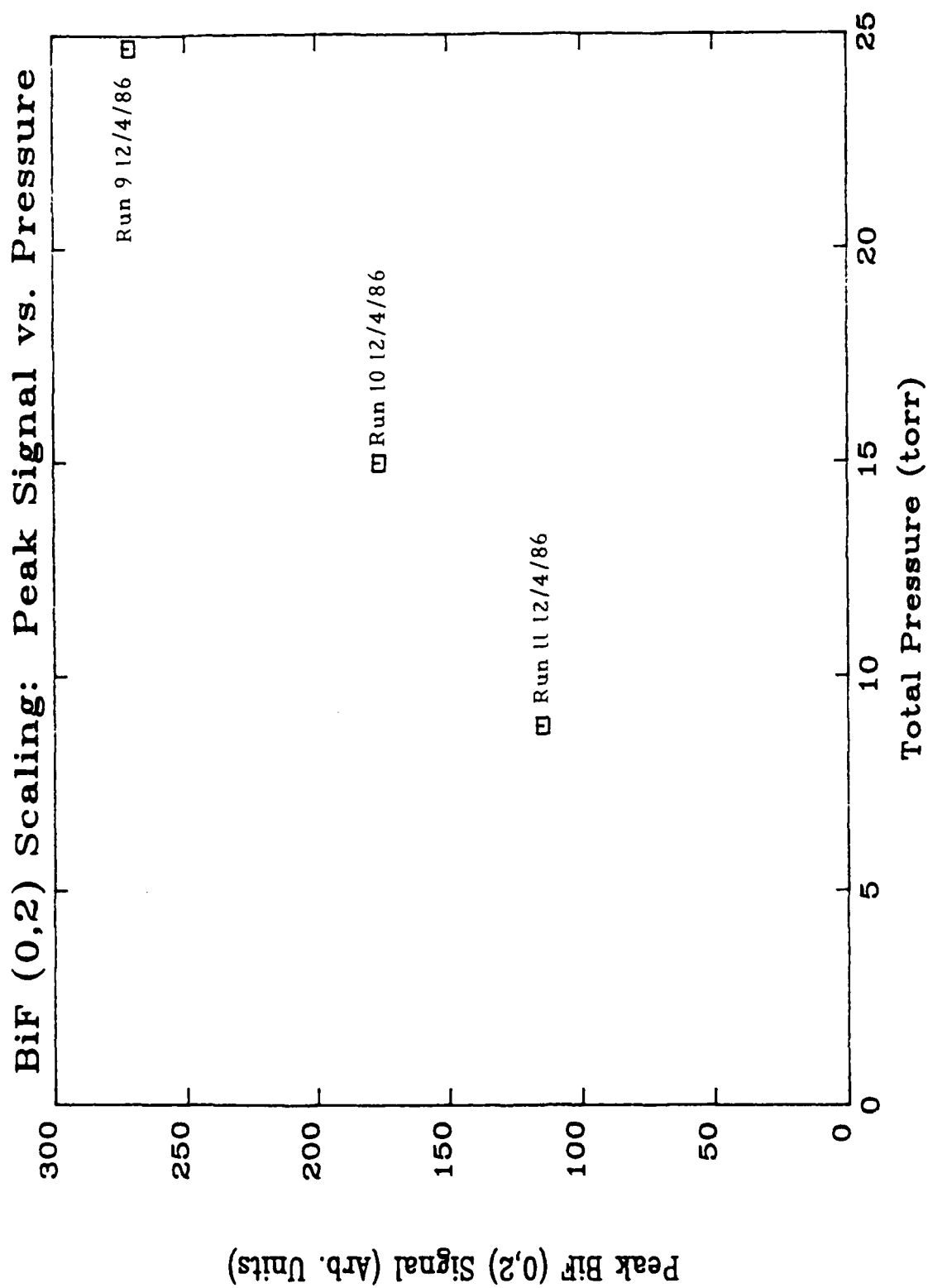


Fig. 20. Peak BiF(0,2) Emission vs. Total Pressure.

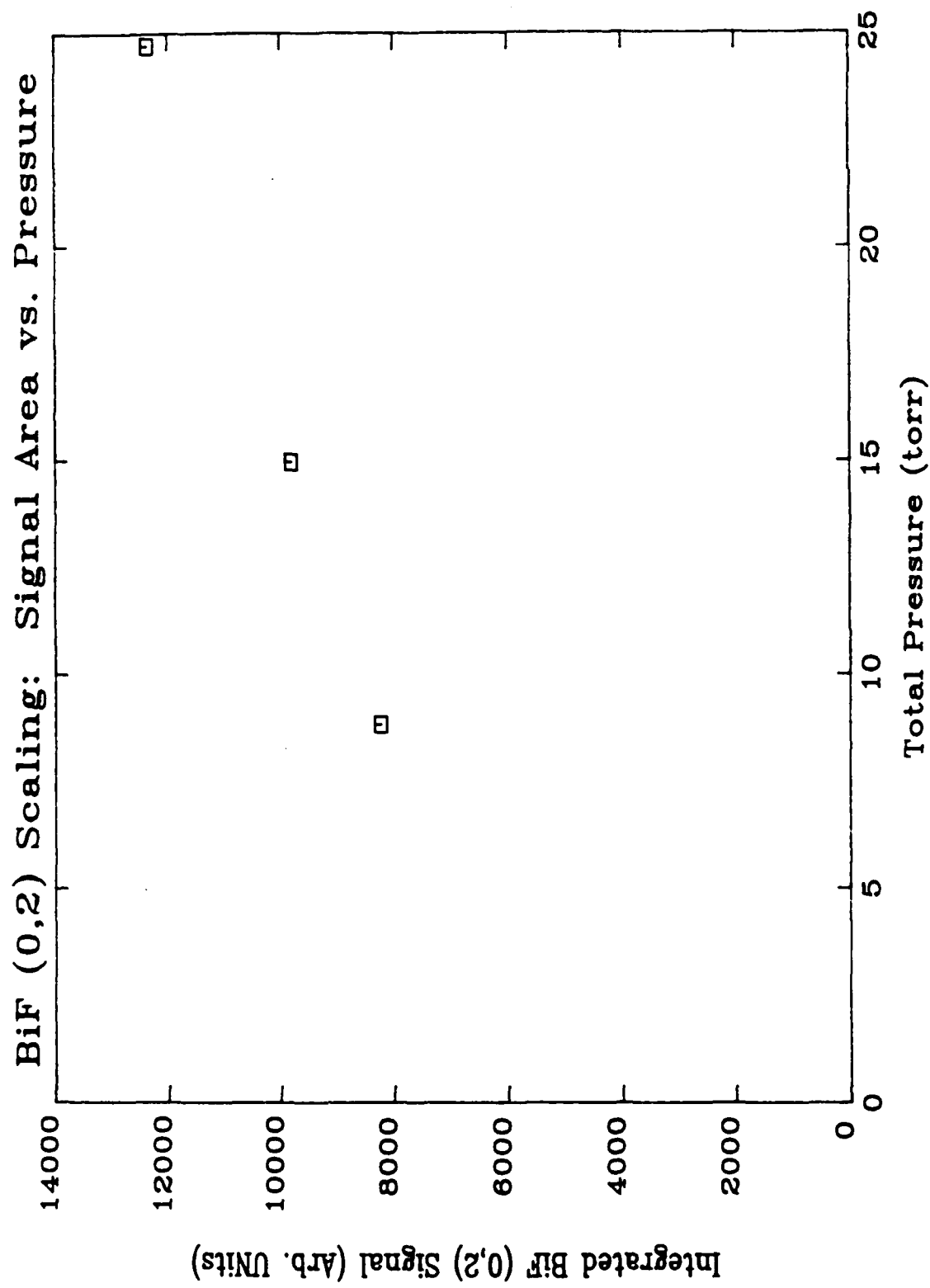


Fig. 21. Integrated BiF(0,2) Emission vs. Total Pressure.

G. EFFECT OF TMB VARIATIONS

In order to optimize the TMB concentration, we measured the $\text{BiF}(A \rightarrow X)$ emission for various concentrations of TMB. The total integrated intensity of BiF increased with TMB up to a TMB concentration of 0.5×10^{15} molecules/cc and decreased at higher concentrations. This is shown in Fig. 22. The cause of the peaking and subsequent decrease of the total emission is not known for certain. TMB is known to quench $\text{Bi}(^2D)$ and $\text{NF}(a^1\Delta)$ rather rapidly; the liberated methyl radicals may also remove these two species that are required to produce $\text{BiF}(A)$.

H. COMMENTS ON THE MEASUREMENTS

Despite the attempts to calibrate the optical components of the system, the detector, the laser, and the gas flows, there is still considerable discrepancy in the value of the $\text{NF}(a^1\Delta)$ density deduced from the fluorescence measurement and the value computed on the basis of the photolysis laser energy and the NF_2 pressure and absorption coefficient. One explanation of the factor of 5.0 discrepancy is the possibility that the high photon flux of the photolysis laser first produces an excited state of NF_2 (i.e., NF_2^*) and then destroys it with the absorption of a second and possibly a third photon. The photolysis of NF_2 does not lead directly to $\text{NF}(a^1\Delta)$ even at low laser power levels¹² since a (50 ± 25) μsec "rise-time" for the emission of $\text{NF}(a^1\Delta)$ is observed, which would be consistent with the formation of a quasi-stable NF_2^* molecule prior to dissociation. The excited molecule of NF_2^* could have a large cross section for the absorption of photons leading to its complete dissociation. According to this hypothesis, one might observe lower $\text{NF}(a^1\Delta)$ densities in a "long pulse" photodissociation than would be predicted on the basis of 20 nsec photolysis of NF_2 /argon mixtures. However, this theory would not explain the low levels of BiF A state in the "laser mixture" photolysis since no fewer F atoms would be created. Our medium is not optically thin, and the absorption of the first photon may lead to the nonlinear absorption of photons near the two ends of the cell with the consequence that fewer

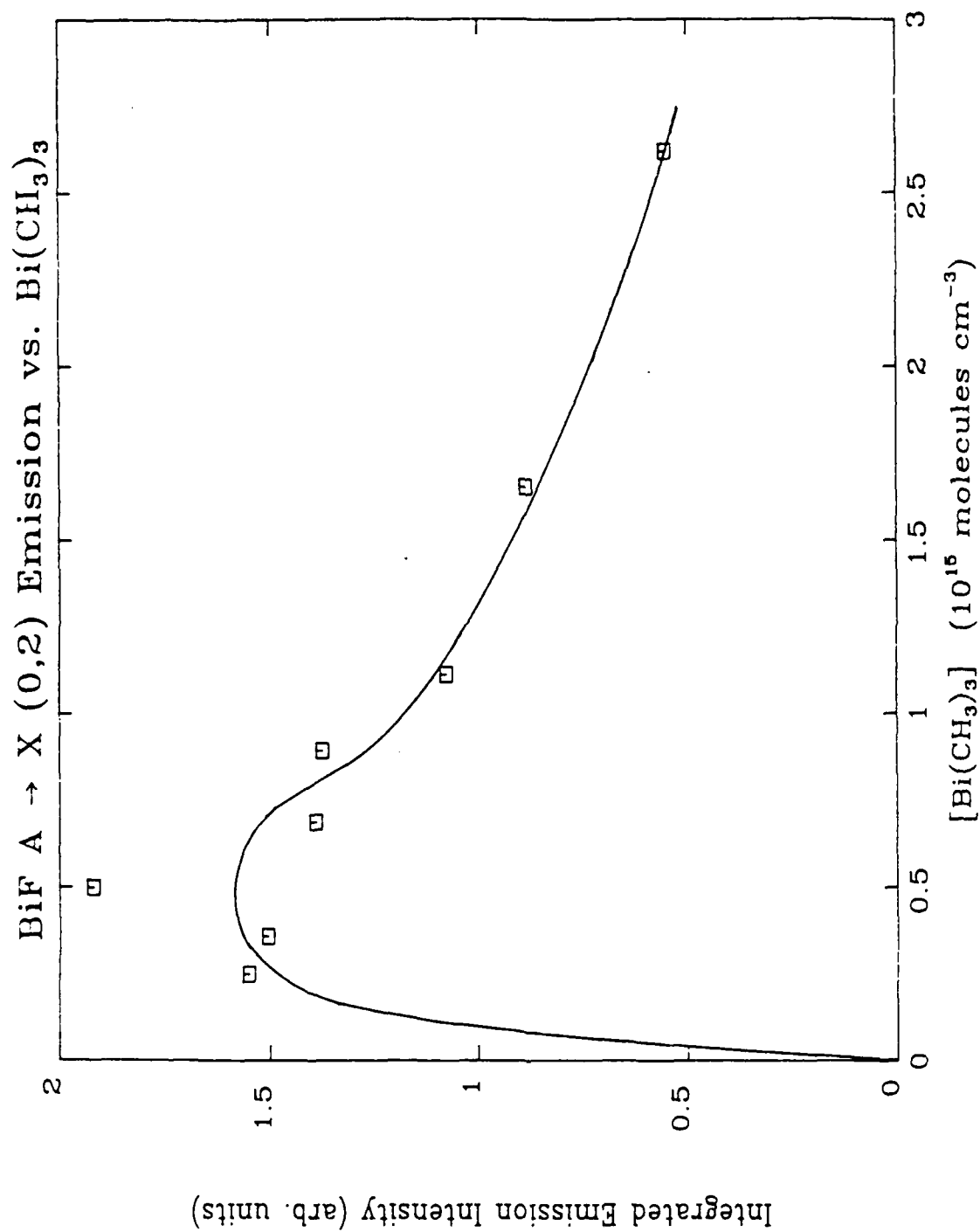


Fig. 22. Integrated BiF(0,2) Emission vs. TMB Density
(Reproduced from Ref. 10.).

photons may reach the center of the cell where the photomultiplier measurements are made. Such a nonlinear absorption process may be even more likely for the TMB, a larger molecule which may have a larger UV multiphoton absorption cross section than does the NF_2 . Observations in the Aerophysics Laboratory that the production of $\text{Bi}(^2\text{D})$ atoms by the 193 nm photolysis of TMB increases nonlinearly with laser power supports this hypothesis. This hypothesis could also account for the peak in the BiF(A) emission plotted versus TMB in Fig. 22, although kinetic limitations may play a role as well.

The effect of the temperature dip in the middle of the flowtube is difficult to assess quantitatively. However, the dip may have caused some recombination of the NF_2 in that portion of the tube with the consequence that the NF_2 density may have been lower in front of the photomultiplier than in the rest of the flowtube. Correcting the calculation for this lower NF_2 density in the N_2F_4 /argon mixture would lower the BiF(A) and $\text{NF(a}^1\Delta)$ densities and bring them into better agreement with the densities determined with the absolute calibrations. However, it probably would not explain the full factor of 5.0 discrepancy. The KrF laser flux was measured, but it is possible that the flux density decreased along the optical path because of divergence of the beam so that we may still be overestimating the laser flux reaching the flowtube. Because of these questions, the densities determined from the photomultiplier measurements with the absolute calibrations may be the most reliable.

The results obtained with SF_6 as a diluent demonstrate that this molecule will be an extremely effective moderator of heat release in any pulsed or premixed laser device concept. For the NF pumped BiF system, laser gains increase as temperatures decrease. The fact that SF_6 is apparently a very slow electronic quencher is also beneficial.

The estimated ground-state production of BiF suggests an empirical value of about 10% for the yield of Bi or BiF products from TMB. This number is used later in Section IV in our modeling discussions.

The scaling of BiF(A) by pressure scaling the reagents suggests that this laser candidate could operate at high densities if the problem of NF_2 and H_2 detonation could be overcome.

IV. MODELING CALCULATIONS

Modeling calculations have been performed for comparison with the present experimental results. A complete model for the photolysis and subsequent chemical reactions in the "laser mixture" includes the photolysis of NF_2 and TMB, the chemical generation of $\text{NF}(a^1\Delta)$, and the production of excited states of bismuth atoms and BiF by transfer processes and chemical reactions. The absorption coefficient of NF_2 at 249 nm, the wavelength of KrF, and the 7% $\text{NF}(a^1\Delta)$ yield are based on studies in this Laboratory.^{12,14} The reactions describing the chemical generation of $\text{NF}(a^1\Delta)$ have been summarized in Ref. 11 and have been used unchanged in the present calculations. The reaction mechanism for $\text{BiF}(A)$ production described in Ref. 11 has been revised on the basis of experimental results of Herbelin⁸ and will be described.

A. MODELING OF THE PHOTOLYSIS OF THE N_2F_4 /ARGON MIXTURE

As mentioned in Section III, the $\text{NF}(a^1\Delta)$ produced by the photolysis of NF_2 in front of the photomultiplier in Run 3 of 11-21-1986 (see Table 1) was calculated from the KrF laser fluence, the NF_2 density and its absorption coefficient, and the quantum yield of $\text{NF}(a^1\Delta)$. Absorption measurements through the NF_2 , N_2F_4 , argon gas mixture indicated an NF_2 density lower than the calculated value by 15%. Temperature probes inserted into the flow tube indicated a total heated length of 84 cm with the laser pulse having to traverse 46 cm of heated gas from one side and 38 cm from the other to reach the position of the photomultiplier. For an absorption cross section¹³ of $6.8 \times 10^{-19} \text{ cm}^2$, the NF_2 density of 2.2×10^{16} molecules/cc attenuates the laser fluence by a factor of 0.51 through the 46 cm path and 0.57 through the 38 cm path. The total laser fluence in the gas volume in front of the photomultiplier was calculated to be 0.22 J/cm^2 from the laser output measurements, the losses in the optical train, and the absorption by the NF_2 . For a 7% quantum yield and an NF_2 density of 2.2×10^{16} , we calculate that an $\text{NF}(a^1\Delta)$ density of 2.8×10^{14} molecules/cc should be produced by the photolysis laser.

This computed density is larger by a factor of 5.0 than the density determined from the measured $\text{NF}(a^1\Delta)$ fluorescence and the absolute calibration of the photomultiplier. The KrF laser fluence which is measured some distance from the flow reactor and corrected for mirror and window losses and NF_2 absorption could account for part of the discrepancy. Experimental verification of the laser fluence nearer to the flowtube would be desirable. A low fluence would affect not only the calculations for the NF_2/argon mixture but also those for the "laser mixture." Another explanation of the low $\text{NF}(a^1\Delta)$ density might be the production of an intermediate excited state of NF_2 by the photolysis and its destruction before it has time to dissociate to $\text{NF}(a^1\Delta)$, NF , and F . The observed risetime of the $\text{NF}(a^1\Delta)$ in these experiments and in those of Ref. 12 cannot be understood in terms of a simple photolysis process. In both studies, the $\text{NF}(a^1\Delta)$ was not produced during the photolysis pulse but over a subsequent time interval of about $(50 \pm 25) \mu\text{sec}$. Keeping these uncertainties in mind, we will proceed with the more complicated modeling of the "laser mixture."

B. MODELING OF THE PHOTOLYSIS OF THE LASER MIXTURE

The kinetic models for the chemical production of $\text{NF}(a^1\Delta)$ and the subsequent production of BiF(A) are listed in Tables 10 and 11. Table 10 does not include all the reactions but only the most important ones. The complete set of reactions can be found in Ref. 11. The BiF reaction mechanism listed in Table 11 is derived from the work of Herbelin and Klingberg.⁷ However, as previously mentioned, a chemical reaction that actually produces the BiF(A) has been substituted for the previously proposed energy transfer process that was thought to create it. The new mechanism is the reaction of $\text{NF}(a^1\Delta)$ with $\text{Bi}(^2\text{D})$ yielding BiF(A) and N atoms.⁸

Table 10. Kinetic Model for $\text{NF}(a^1\Delta)$

Photoinitiation	$\text{NF}_2 + h\nu$	+	$\text{NF}(a,X) + \text{F}$
	$\text{Bi}(\text{CH}_3)_3 + h\nu$	+	$\text{Bi} + 3\text{CH}_3$
Pumping reactions	$\text{F} + \text{H}_2$	+	$\text{HF} + \text{H}$
	$\text{H} + \text{NF}_2$	+	$\text{HF} + \text{NF}(a,X)$
F atom regeneration	$2\text{NF}(X)$	+	$\text{N}_2 + 2\text{F}$
Chain termination	$\text{F} + \text{NF}_2 + \text{M}$	+	$\text{NF}_3 + \text{M}$
Other loss processes	$\text{H} + \text{NF}(a^1\Delta)$	+	$\text{HF} + \text{N}$
	$\text{N} + \text{NF}(a^1\Delta)$	+	$\text{N}_2 + \text{F}$
	$\text{SF}_6 + \text{NF}(a^1\Delta)$	+	$\text{SF}_6 + \text{NF}$
	$\text{N} + \text{NF}_2$	+	2NF
	$\text{TMB} + \text{NF}(a^1\Delta)$	+	$\text{TMB} + \text{NF}$

Table 11. Kinetic Processes Involving Bi and BiF

BiF(A) pumping	NF(a) + Bi(S)	+	NF(X) + Bi(² D)	1.9×10^{-10}
	NF(a) + Bi(² D)	+	N + BiF(A)	2.0×10^{-10}
Recycling of ground state	BiF(X) + H	+	Bi(S) + HF	4.0×10^{-11}
Collisional removal of BiF(A)	BiF(A) + SF ₆	+	BiF(X) + SF ₆	4.5×10^{-13}
	BiF(A) + NF(a)	+	Bi(² D) + NF ₂	1.0×10^{-10}
	BiF(A) + H	+	Bi(² D) + HF	4.0×10^{-11}
	BiF(A) + NF ₂	+	Bi(S) + NF ₃	1.0×10^{-10}
Miscellaneous reactions	Bi(² D) + NF ₂	+	BiF(X) + NF	5.0×10^{-12}
Vibrational relaxation	BiF(X,v) + SF ₆	+	BiF(X,v-1) + SF ₆	$\geq 1.0 \times 10^{-11}$
Spontaneous emission	BiF(A)	+	BiF(X) + hν	7.5×10^5

The first part of the modeling is the calculation of the photolysis of the NF₂ and the TMB. The KrF laser fluence for Run 1 of November 26, 1986 (Table 1) was 0.60 J/cm² at the entrance to the optical train. This fluence was reduced by an estimated factor of 0.37 in the upstream leg by two mirror reflections and the Brewster angle window and by a factor of 0.54 in the downstream leg. Therefore, a laser fluence of 0.22 J/cm² entered the gas from the upstream side and 0.32 J/cm² entered from the downstream

side. TMB has an absorption cross section¹⁸ of $4.0 \times 10^{-18} \text{ cm}^2$ at 249 nm, which is a factor of 6 larger than the value of 6.8×10^{-19} for NF_2 . However, the initial concentration is a factor of 25 lower than that of the NF_2 so the TMB should account for only about 20% of the absorption. The difficulty with this calculation is that the details of the TMB photolysis are not known. One photon at 249 nm is not sufficient to fully dissociate TMB to Bi atoms, although excited TMB or its photofragments may decompose or react easily with other constituents to release bismuth atoms. Alternatively, the bismuth may be released by sequential photon absorption. We assume that the excited state of TMB (or its photofragments) is not a large sink of photons (CH_3 does not absorb), but this is not known for certain. The data of Klingberg and Herbelin⁷ indicate a 3% total yield of bismuth from TMB in their flow tube. Herbelin reported a 10 to 15% yield in Ref. 8. We will treat the bismuth yield as a parameter with a nominal value of 10%.

The photolysis calculation takes into account the decrease in the NF_2 density along the length of the flowtube during the laser pulse and the consequent effect on the laser fluence reaching the position of the photomultiplier. According to our calculations, 26% of the NF_2 is dissociated at the position of the photomultiplier. A smaller fraction would be calculated if the TMB or its products were assumed to absorb more than one photon.

The products of the photolysis^{12,14} are 0.93 NF, 0.07 $\text{NF}(a^1\Delta)$, and 1 F atom for each NF_2 dissociated. In their study of NF_2 photolysis, Koffend et al.¹² observed that $\text{NF}(a^1\Delta)$ did not appear immediately but had a risetime of about $(50 \pm 25) \text{ } \mu\text{sec}$. This risetime is consistent with the observations in the present study. We assume in the baseline calculations that the F atoms and ground state NF are produced promptly, although some calculations have also been performed to determine the effect of a delayed production. Recent evidence¹⁴ shows that $\text{NF}(X)$ production is prompt; in addition, the quantum yield of F (and presumably $\text{NF}(X)$) per photon absorbed by NF_2 has been measured to be unity.

Because of uncertainty in the mechanism of TMB photolysis, the methyl radical production is unknown. Methyl radicals can react with F atoms and NF_2 or recombine to form C_2H_6 . F atoms can probably attack the TMB and its photofragments, thus reducing their reactions with H_2 . Such chemical reactions may liberate more bismuth than the direct photolysis of TMB. In any case, some F and H atoms are removed in processes involving methyl radicals, TMB, and ethane that form HF as a product. However, the concentration of TMB is low enough that the removal of H and F atoms should not be a dominant effect even if all the methyl radicals are available for reaction. The postphotolysis gas composition is listed in Table 1 for Run 1 of November 26 except that the NF_2 is partially photolyzed as previously described, and each TMB is replaced with three methyl radicals and 0.1 bismuth atom.

A sample calculation is shown in Table 12. The $\text{NF}(a^1\Delta)$ and $\text{BiF}(A)$ concentrations peak between 8 and 10 μsec . This is the time required for H atoms, which form in 2 to 3 μsec by the reaction of F atoms with H_2 , to react with the NF_2 and produce $\text{NF}(a)$. At longer times, electronic excitation is removed from the gas mixture by loss processes such as spontaneous emission of the $\text{BiF}(A)$ and reactions/quenching of $\text{NF}(a)$ by TMB, N atoms, and H atoms. For an assumed bismuth yield of 10% of the TMB, we calculate the maximum $\text{BiF}(A, v = 0)$ to be 3.4×10^{12} molecules/cc. This, however, is a factor of 24 larger than the experimental value of 1.4×10^{11} determined on the basis of an absolute calibration of the photomultiplier; it is a factor of 5 larger than the experimental value of 7.0×10^{11} determined with the photomultiplier calibrated relative to $\text{NF}(a^1\Delta)$ emission.

Since the bismuth yield is uncertain, calculations were performed for several concentrations of bismuth atoms, and the maximum $\text{BiF}(A)$ concentrations are plotted in Fig. 23. The $\text{BiF}(A)$ is linear with bismuth at low concentrations where $\text{NF}(a^1\Delta)$ is not seriously affected by its presence. Also plotted in Fig. 23 is the concentration of $\text{BiF}(X, v = 0)$ at 20 μsec , which is also proportional to the bismuth concentration. Therefore, the ratio of $\text{BiF}(A)$ to $\text{BiF}(X)$ is fairly independent of the initial bismuth atom concentration.

Table 12. Sample Code Calculation for "Laser" Mixture

LN8IF14
REVISED FEB 2, 1987

NF-BIF RUN #1 26 NOV 88
22-Jul-87
08:23 AM

SF8 = .280089E+18
NF2 = .931517E+16
NF = .294561E+16
NF2A = 0 This is the NF+ precursor. Tau = 0 microsec
NF10 = .32729E+15
F = .32729E+16
H2 = .131904E+17
BiF = 0
Bi0 = .554116E+14
TMB = 0
CH3 = .186235E+16
Assumes Boltzmann distribution over BiF(300).
Calculates vibrational distribution in BiF(X).
Assumes 2.5E+5 Joules/mole of photons
Power in units of watts/cc. Energy (total) in units of Joules/cc.

Temperature = 414 K - variable
NF2 Dissociation = 28 %
Standard Rates --
Zero power gain, Bi Source is Bi0 = 0.1 x nominal TMB
GAIN2 is the gain on A,0 to X,v=2
GAIN3 is the gain on A,0 to X,v=3
H ATOM REMOVAL BY CH3
i.e. 3 x the nominal TMB.

TIME	Bi0	Bi1	BIF000	BIF001	BIF002	BIF003	BIF300V0	CH3	CH4	GAIN2	GAIN3
0.0	5.54E+13	0.00E+00	0.00E+00	0.00E+00	0.00E+00	0.00E+00	0.00E+00	1.68E+15	0.00E+00	0.00E+00	0.00E+00
2.0	4.52E+13	5.12E+12	4.05E+12	6.14E+11	1.09E+11	1.90E+10	2.23E+11	1.50E+15	1.61E+14	4.54E-05	4.07E-05
4.0	3.48E+13	9.92E+12	7.51E+12	1.43E+12	2.86E+11	5.25E+10	1.03E+12	1.28E+15	3.83E+14	2.95E-04	1.94E-04
6.0	2.50E+13	1.25E+13	1.17E+13	2.50E+12	5.34E+11	1.02E+11	2.26E+12	1.10E+15	5.59E+14	6.83E-04	4.27E-04
8.0	1.73E+13	1.21E+13	1.68E+13	3.79E+12	8.30E+11	1.64E+11	3.12E+12	9.72E+14	6.91E+14	9.12E-04	5.89E-04
10.0	1.20E+13	1.01E+13	2.23E+13	5.07E+12	1.12E+12	2.29E+11	3.28E+12	8.75E+14	7.87E+14	6.58E-04	6.07E-04
12.0	8.46E+12	7.81E+12	2.71E+13	6.17E+12	1.37E+12	2.88E+11	2.92E+12	8.05E+14	8.57E+14	6.16E-04	5.24E-04
14.0	6.19E+12	5.91E+12	3.09E+13	7.05E+12	1.58E+12	3.40E+11	2.38E+12	7.58E+14	9.06E+14	3.19E-04	4.07E-04
16.0	4.67E+12	4.49E+12	3.36E+13	7.73E+12	1.75E+12	3.85E+11	1.87E+12	7.23E+14	9.40E+14	4.76E-05	2.90E-04
18.0	3.82E+12	3.46E+12	3.56E+13	8.25E+12	1.89E+12	4.25E+11	1.45E+12	7.00E+14	9.62E+14	-1.8E-03	2.05E-04
20.0	2.88E+12	2.72E+12	3.70E+13	8.68E+12	2.01E+12	4.60E+11	1.14E+12	6.86E+14	9.77E+14	-3.5E-03	1.34E-04
22.0	2.34E+12	2.19E+12	3.79E+13	8.99E+12	2.12E+12	4.93E+11	8.98E+11	6.77E+14	9.86E+14	-4.9E-03	8.07E-05
24.0	1.93E+12	1.79E+12	3.88E+13	9.28E+12	2.21E+12	5.24E+11	7.22E+11	6.72E+14	9.90E+14	-5.9E-03	3.95E-05
26.0	1.62E+12	1.49E+12	3.91E+13	9.49E+12	2.30E+12	5.62E+11	5.90E+11	6.70E+14	9.93E+14	-6.8E-03	7.49E-06
28.0	1.38E+12	1.26E+12	3.94E+13	9.68E+12	2.37E+12	5.79E+11	4.89E+11	6.69E+14	9.93E+14	-7.5E-03	1.8E-04
30.0	1.19E+12	1.08E+12	3.98E+13	9.85E+12	2.44E+12	6.04E+11	4.11E+11	6.69E+14	9.93E+14	-8.1E-03	-3.8E-04
32.0	1.04E+12	9.34E+11	3.98E+13	1.00E+13	2.51E+12	6.28E+11	3.50E+11	6.71E+14	9.92E+14	-8.6E-03	-5.5E-04
34.0	9.10E+11	8.19E+11	3.99E+13	1.01E+13	2.57E+12	6.50E+11	3.02E+11	6.72E+14	9.90E+14	-9.0E-03	-6.9E-04
36.0	8.14E+11	7.24E+11	3.99E+13	1.02E+13	2.63E+12	6.72E+11	2.63E+11	6.74E+14	9.88E+14	-9.4E-03	-8.1E-04
38.0	7.29E+11	6.46E+11	3.99E+13	1.04E+13	2.68E+12	6.93E+11	2.31E+11	6.76E+14	9.86E+14	-9.8E-03	-9.2E-04
40.0	6.56E+11	5.81E+11	4.00E+13	1.05E+13	2.73E+12	7.12E+11	2.05E+11	6.78E+14	9.84E+14	-1.0E-02	-1.0E-03
22-Jul-87 08:24 AM											

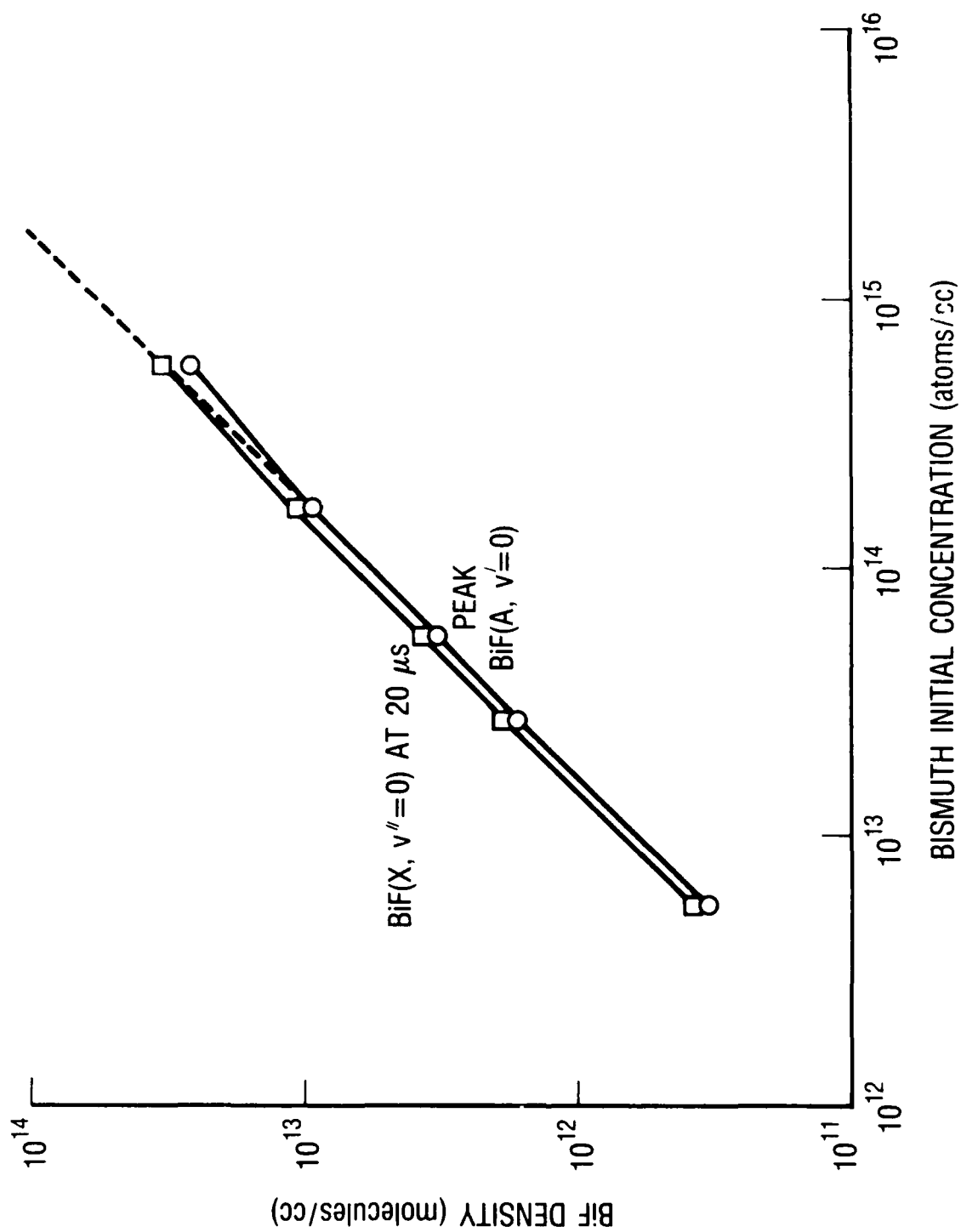


Fig. 23. Modeling Predictions of Peak $\text{BiF}^+(A)$ and $\text{BiF}(X)$ Densities vs. Initial Bismuth Atoms.

In the previous section, the $\text{NF}(a^1\Delta)$ concentration calculated for the $\text{NF}_2/\text{N}_2\text{F}_4$ argon mixture was larger than the measured concentration by a factor of 5.0. One possible explanation of this discrepancy might be that the laser fluence was lower than we calculated even after taking into account the degradation of the optics between the flowtube and the excimer laser. To examine the consequences of various laser fluences, calculations were performed for a range of initial fractions of photolyzed NF_2 . The calculated maximum concentrations of $\text{BiF}(A,0)$ are plotted in Fig. 2 versus fraction of NF_2 photolyzed. There is a broad maximum around the nominal operating condition of 50%. However, the maximum $\text{BiF}(A,0)$ falls off almost linearly at the lower levels of initiation. A maximum $\text{BiF}(A,0)$ of 6.5×10^{11} molecules/cc is calculated when the level of initiation (the fraction of photolyzed NF_2) is reduced by a factor of 5 to 0.052. This maximum is reduced further to about 4.6×10^{11} if we take into account the A state vibrational temperature of 900 K measured with the OMA. This calculated value is a factor of 3 larger than the concentration measured with the absolutely calibrated photomultiplier. The measurements in the $\text{NF}_2/\text{N}_2\text{F}_4$ argon mixture and in the "laser mixture" are consistent in that they agree with the modeling calculations only if we assume (1) a significantly lower laser fluence than that recorded in the experiments, (2) a low yield of product F and NF from NF_2 photolysis, or (3) a systematic error in the absolute calibration.

The calculated concentration of $\text{BiF}(X, v = 0)$, the ground state of BiF, is not very sensitive to the level of initiation, at least at the lower levels. At the lower initiation levels, the $\text{BiF}(X)$ is produced more slowly, but there are fewer H atoms for its removal. The values calculated for time = 20 μsec are plotted in Fig. 2 versus the fraction of NF_2 photolyzed. We have assumed a 10% yield of bismuth atoms from the TMB to be consistent with the OMA spectral absorption measurements from which a $\text{BiF}(X)$ concentration of 5×10^{13} molecules/cc was deduced. Therefore, the OMA measurements do not settle the question of the laser fluence, but they do help establish the populations of bismuth atoms.

The initial concentration of TMB was optimized for BiF(A) production in experiments in which the laser fluence was kept fixed and the TMB was varied. It was found that the integrated intensity of BiF(A) peaked at a TMB density of about 0.5×10^{15} molecules/cc and decreased at higher levels of TMB (Fig. 22).

One explanation of this decrease of BiF(A) at high TMB densities might be the removal of excited species by the TMB. TMB removes $\text{NF}(a^1\Delta)^{19}$ and $\text{Bi}(^2\text{D})^{20}$ with rate coefficients of 2.7×10^{-11} cc/molecule-sec and 7.8×10^{-11} cc/molecule-sec, respectively. CH_3 radicals may also quench $\text{NF}(a^1\Delta)$ and $\text{Bi}(^2\text{D})$ (preliminary $k_{\text{CH}_3} = 2.6 \times 10^{-10}$ cc/molecule-sec). In addition, the methyl radicals liberated by the TMB (and perhaps the TMB itself) will remove both H and F atoms resulting in the formation of HF. Although there is initially 30 times as much NF_2 as TMB in the gas mixture, there are only 10 times as many NF_2 molecules as potential methyl radicals competing for the H atoms.

Another possible contribution to the decrease of BiF(A) at high TMB densities is nonlinear absorption of the photolysis laser photons by the TMB. Preliminary absorption measurements in the Aerophysics Laboratory²⁰ suggest that $\text{Bi}(^2\text{D})$ production increases nonlinearly with laser power. This could mean that the absorption cross section of TMB in the present "laser mixture" experiments could be significantly larger, particularly at the two entrances to the reactor cell. Therefore, the laser flux actually reaching the center of the cell (where we make the photomultiplier measurements) could be greatly attenuated and much lower than we have used in the kinetic modeling calculations. If we assume that the integrated intensity peaks in Fig. 22 because of the attenuation of the photolysis laser by single and multiphoton processes, we can calculate an effective cross section of 3.3×10^{-17} cm² from the density of TMB (0.5×10^{15} molecules/cc) at the peak and the distance of the photomultiplier from the end of the cell (60 cm). However, this is a factor of 8 larger than the absorption coefficient reported in Ref. 18. An absorption coefficient of 4.5×10^{-18} cm² for TMB at 248.5 nm was measured in a Beckman Spectrophotometer in the

Aerophysics Laboratory. This is in good agreement with the value of $4.0 \times 10^{-18} \text{ cm}^2$ of Ref. 18.

In the present experiments, the maximum BiF(A) signal was observed to decrease with larger laser fluence. This would be expected if the laser fluence were large enough to dissociate substantially more than 60% of the NF_2 (Fig. 2). However, this is inconsistent with the postulate of low laser fluence and, therefore, low fractional dissociation of NF_2 . According to the calculated values plotted in Fig. 2, the BiF(A) should increase with NF_2 dissociation at our lower than expected laser fluence. One possibility is that we are not correctly accounting for the attack of $\text{NF}(a^1\Delta)$ and BiF(A) by methyl radicals produced in the dissociation of TMB.

In addition, the decrease of the maximum BiF(A) signal with larger laser fluences is consistent with the hypothesis of nonlinear absorption of TMB. At the higher laser fluences, increased absorption of photons by the TMB at the ends of the cell could actually decrease the fractional photon fluence reaching the center of the cell. A better knowledge of the photolysis of TMB and its absorption of photons is one of the first requirements of more reliable modeling of the present experiments.

V. ASSESSMENT AND DISCUSSION

The peak concentration of BiF(A) determined with the calibrated photomultiplier measurements was significantly lower than expected but could be increased with several changes in the apparatus. The heated cell should be closed more tightly to avoid temperature gradients in the vicinity of the photomultiplier measurements. The optical train should be repaired and periodically checked to ensure the delivery of the photolysis laser flux. Also, a scheme should be devised to allow the measurement of the laser flux near the cell window instead of upstream in the optical train. Higher laser fluxes could be considered to provide a larger initial concentration of F atoms. The absorption of the NF₂ prevents much increase in the NF₂ pressure unless the tube length is reduced or transverse photolysis geometry is used.

The ability to scale the reagents linearly suggests that this laser candidate could operate at high densities if the problem of NF₂ and H₂ detonation could be overcome. However, scaling the pressure of the TMB relative to NF₂ and H₂ does not appear to increase the BiF(A).

Uncertainties in the kinetics could account for some of the discrepancy in the measured concentrations and the code predictions. Of importance to understanding the present experiment are the photophysics issues of the F and NF yield per absorbed photon in the photolysis of NF₂, as well as the production of NF(a¹Δ) in the photolysis of NF₂ with long-pulse, high-power lasers. Two separate studies in the Aerophysics Laboratory are in progress to investigate kinetics and photophysics questions that could affect the model predictions. These studies will include subtasks that may provide solutions to further scaling in such a demonstration device. It is clear that the photolysis of TMB needs to be studied and understood.

One solution to two experimental difficulties in the current work is the addition of a hydrogen bearing molecule HX, such as HI or HBr. Such an addition would allow the prompt generation of H atoms from ultraviolet photolysis, thus eliminating one reaction step, Reaction 4. Furthermore,

such molecules could serve to stabilize the mixtures and suppress detonation by scavenging free radicals such as F atoms. If such detonation control is successful, then pressuring scaling could indeed be achieved to pressure much higher than presently possible. However, using HI or HBr would preclude running on the NF_2/H_2 chain.

REFERENCES

1. J. M. Herbelin and N. Cohen, Chem. Phys. Lett. 20, 605 (1973).
2. R. J. Malins and D. W. Setser, J. Phys. Chem. 85, 1342 (1981).
3. C. T. Cheah and M.A.A. Clyne, J.C.S. Faraday II, 76 1543 (1980).
4. G. A. Capelle, D. G. Sutton, and J. I. Steinfeld, J. Chem. Phys. 69, 5140 (1978).
5. J. M. Herbelin, R. R. Giedt, and H. A. Bixler, J. Applied Phys. 54, 28 (1983).
6. M. A. Kwok, J. M. Herbelin, R. R. Giedt, and W. R. Warren, Jr., "Supersonic Flows for the Production of High NF(a¹ Δ) Densities," A.I.A.A./ S.D.I.O. High Power Laser Device Conference, March 2-4, 1987.
7. J. M. Herbelin and R. A. Klingberg, Int. J. Chem. Kinet. 16, 849 (1984).
8. J. M. Herbelin, "Efficient Production of Electronically Excited BiF(AO⁺) Via Collisions with NF(a). II.," Proceedings of the International Conference on Lasers 86, ed. W. B. Lacina, Soc. for Opt. and Quantum Electronics, STS Press. 281 (1987).
- 9a. R. F. Heidner, H. Helvajian, J. S. Holloway, and J. B. Koffend, J. Chem. Phys. 84, 2137 (1986).
- 9b. H. Helvajian, J. S. Holloway, and J. B. Koffend, J. Chem. Phys. (in press).
10. J. B. Koffend and R. F. Heidner, Time-Resolved Kinetics of the NF*-BiF Candidate Chemical Laser System, TOR-0086(6604)-1, The Aerospace Corporation, El Segundo, Ca. (30 September 1986).
11. J. F. Bott, NF-BiF Laser Modeling, TR-0086(6930-01)-12, The Aerospace Corporation, El Segundo, Ca. (20 June 1986).
12. J. B. Koffend, C. E. Gardner, and R. F. Heidner, J. Chem. Phys. 83, 2904 (1985).
13. R. F. Heidner, H. Helvajian, and J. B. Koffend, J. Chem. Phys. 87, 520 (1987).
14. R. F. Heidner, H. Helvajian, J. S. Holloway, and J. B. Koffend, "Direct Observation of NF(X) Using Laser Induced Fluorescence: NF

Ground State Vibrational Kinetics and Determination of the $H + NF_2$ Branching Ratio," AIAA Thermophysics, Plasmadynamics and Lasers Conference, June 27-29, 1988, San Antonio, Texas.

15. J. F. Bott, The Quantum Yield of $NF(a)$ in NF_2 Photolysis, TR-0086A(2604)-1, The Aerospace Corporation, El Segundo, Ca. (4 November 1987).
16. W. E. Jones and T. D. McLean, J. Mol. Spec. 90, 481 (1981).
17. H. Helvajian, et al., Vibrational Relaxation and Electronic Quenching-Rate Coefficients for $BiF(AO^+, v')$ by SF_6 , TR-0088(3604)-1, The Aerospace Corporation, El Segundo, Ca. (22 August 1988).
18. J. Connor, P. J. Young, and O. P. Strausz, J. Am. Chem. Soc. 91, 7687 (1969) and 93, 822 (1971).
19. D. W. Setser (personal communication) (May 1988).
20. H. Helvajian and J. B. Koffend, (personal communication) (July 1988)

LABORATORY OPERATIONS

The Aerospace Corporation functions as an "architect-engineer" for national security projects, specializing in advanced military space systems. Providing research support, the corporation's Laboratory Operations conducts experimental and theoretical investigations that focus on the application of scientific and technical advances to such systems. Vital to the success of these investigations is the technical staff's wide-ranging expertise and its ability to stay current with new developments. This expertise is enhanced by a research program aimed at dealing with the many problems associated with rapidly evolving space systems. Contributing their capabilities to the research effort are these individual laboratories:

Aerophysics Laboratory: Launch vehicle and reentry fluid mechanics, heat transfer and flight dynamics; chemical and electric propulsion, propellant chemistry, chemical dynamics, environmental chemistry, trace detection; spacecraft structural mechanics, contamination, thermal and structural control; high temperature thermomechanics, gas kinetics and radiation; cw and pulsed chemical and excimer laser development including chemical kinetics, spectroscopy, optical resonators, beam control, atmospheric propagation, laser effects and countermeasures.

Chemistry and Physics Laboratory: Atmospheric chemical reactions, atmospheric optics, light scattering, state-specific chemical reactions and radiative signatures of missile plumes, sensor out-of-field-of-view rejection, applied laser spectroscopy, laser chemistry, laser optoelectronics, solar cell physics, battery electrochemistry, space vacuum and radiation effects on materials, lubrication and surface phenomena, thermionic emission, photo-sensitive materials and detectors, atomic frequency standards, and environmental chemistry.

Computer Science Laboratory: Program verification, program translation, performance-sensitive system design, distributed architectures for spaceborne computers, fault-tolerant computer systems, artificial intelligence, micro-electronics applications, communication protocols, and computer security.

Electronics Research Laboratory: Microelectronics, solid-state device physics, compound semiconductors, radiation hardening; electro-optics, quantum electronics, solid-state lasers, optical propagation and communications; microwave semiconductor devices, microwave/millimeter wave measurements, diagnostics and radiometry, microwave/millimeter wave thermionic devices; atomic time and frequency standards; antennas, rf systems, electromagnetic propagation phenomena, space communication systems.

Materials Sciences Laboratory: Development of new materials: metals, alloys, ceramics, polymers and their composites, and new forms of carbon; non-destructive evaluation, component failure analysis and reliability; fracture mechanics and stress corrosion; analysis and evaluation of materials at cryogenic and elevated temperatures as well as in space and enemy-induced environments.

Space Sciences Laboratory: Magnetospheric, auroral and cosmic ray physics, wave-particle interactions, magnetospheric plasma waves; atmospheric and ionospheric physics, density and composition of the upper atmosphere, remote sensing using atmospheric radiation; solar physics, infrared astronomy, infrared signature analysis; effects of solar activity, magnetic storms and nuclear explosions on the earth's atmosphere, ionosphere and magnetosphere; effects of electromagnetic and particulate radiations on space systems; space instrumentation.